

The ROSAT Galactic Plane Survey: analysis of a low latitude sample area in Cygnus^{*}

C. Motch^{1,2}, P. Guillout¹, F. Haberl², M. Pakull¹, W. Pietsch², and K. Reinsch³

¹ Observatoire Astronomique, UA 1280 CNRS, 11 rue de l'Université, F-67000 Strasbourg, France

² Max-Planck-Institut für Extraterrestrische Physik, D-85748, Garching bei München, Germany

³ Sternwarte, Geismarlandstrasse 11, D-37083, Göttingen, Germany

Received 20 March 1996 / Accepted June 1996

Abstract. We present the analysis of the point source content of a low galactic latitude region selected from the ROSAT all-sky survey. The test field is centered at $l = 90^\circ$, $b = 0^\circ$ and has an area of 64.5 deg^2 . A total of 128 soft X-ray sources are detected above a maximum likelihood of 8. Catalogue searches and optical follow-up observations show that in this direction of the galactic plane, 85% of the sources brighter than $0.03 \text{ PSPC cts s}^{-1}$ are identified with active coronae. F-K type stars represent 67% ($\pm 13\%$) of the stellar identifications and M type stars account for 19% ($\pm 6\%$). A small but significant number of X-ray sources are associated with A type stars on the basis of positional coincidence. These results together with those of similar optical campaigns demonstrate that the soft X-ray population of the Milky Way is largely dominated by active stars. We show that the density and distribution in flux and spectral type of the active coronae detected in X-rays are consistent with the picture drawn from current stellar population models and age dependent X-ray luminosity functions. The modelling of this population suggests that most of the stars detected by ROSAT in this direction are younger than 1 Gyr. This opens the possibility to extract in a novel way large samples of young stars from the ROSAT all-sky survey. The small number of unidentified sources at low X-ray flux put rather strong constraints on the hypothetical X-ray emission from old neutron stars accreting from the interstellar medium. Our observations clearly rule out models which assume no dynamical heating for this population and a total number of $N_{\text{ns}} = 10^9$ neutron stars in the Galaxy. If accretion on polar caps is the dominant mode then our upper limit may imply $N_{\text{ns}} \approx 10^8$. Among the non coronal identifications are three white dwarfs, a Seyfert 1 active nucleus, two early type stars and one cataclysmic variable. We also

report the discovery of a Me + WD close binary system with $P_{\text{orb}} \approx 12 \text{ h}$.¹

Key words: X-ray general, X-ray stars, stars: activity, stars: neutron, stars: statistics

1. Introduction

Starting in 1990 July the ROSAT X-ray satellite has performed during six months the first soft X-ray all-sky survey ever made with an imaging instrument. At this occasion, the position sensitive proportional counter (PSPC) was moved in the focal plane of the X-ray telescope (XRT). This detector offers an energy range of 0.1-2.4 keV and an energy resolution of about 45% at 1 keV. In survey mode, the satellite was scanning the sky in great circles perpendicular to the solar direction thus covering the whole celestial sphere in six months time. The spin period of the satellite was synchronized with its orbital motion. Any part of the sky was continuously seen during a maximum detector crossing time of 32 s every 96 min. The time interval during which a given source is visible mainly depends upon its ecliptic latitude and the cumulative exposure time varies between 300 sec and 40,000 sec for the equatorial and polar regions respectively. The mean flux sensitivity is $\approx 2 \cdot 10^{-13} \text{ erg cm}^{-2} \text{ s}^{-1}$ (0.1-2.4 keV). Taking into account the varying point spread function across the PSPC field of view, the final spatial resolution of the survey is of the order of $1.5'$ with a capability to localize point sources with a 1σ accuracy close to $20''$. A review of the main characteristics of the ROSAT satellite and instrumentation can be found in Trümper (1983) and Pfeffermann et al. (1986) while the ROSAT all-sky survey (RASS) is described in Voges (1992).

Send offprint requests to: C. Motch

^{*} Partly based on observations obtained at the Observatoire de Haute-Provence, CNRS, France

¹ Tables 11 and 12 are also available in electronic form at the CDS via anonymous ftp cdsarc.u-strasbg.fr

As part of the RASS the plane of the Galaxy was also surveyed entirely. The analysis of the region of the sky located below absolute galactic latitude 20° , known as the ROSAT Galactic Plane Survey (RGPS) is the scope of a distinct project (Motch et al. 1991). Over 14,000 XRT survey sources are found in the Milky Way, most of these being unknown before the launch of ROSAT.

As for studies at high galactic latitudes, the RGPS source catalogue will serve as basis for statistical analysis of various kinds of X-ray emitters. The galactic plane is suited for studies of active coronae, OB stars and cataclysmic variables for instance. It will also be extremely useful as finder for follow-up observations of particularly interesting objects in the forthcoming years. The RGPS may also specifically address several pending questions of high astrophysical interest such as the origin of the hard X-ray galactic ridge emission, the nature of supersoft X-ray sources and the evolutionary status of accreting binary sources for example.

Compared with previous X-ray surveys of the Galaxy, the RGPS offers a much larger area and improved sensitivity and spatial resolution. The Einstein observatory mapped only $\approx 2.5\%$ of the Galactic Plane (Hertz & Grindlay 1984, 1988) at a flux limit similar to that of ROSAT while the previous Milky Way surveys performed with collimating instruments (e.g., HEAO: Nugent et al. 1983, Wood et al. 1984, EXOSAT: Warwick et al. 1985) had a sensitivity a factor 10 to 100 lower than that of the RGPS.

Obviously, the identification of this large amount of X-ray sources is far beyond the nowadays possibilities. Accordingly, we used three different paths for exploring this unprecedented amount of new sources. The first and easiest step was the cross correlation of RGPS source positions with astronomical catalogues, mostly extracted from the SIMBAD database. The historical development of astronomy has favoured galactic studies and the number of Milky Way objects held in catalogues is rather large. With the positional accuracy of the survey, up to 30% of RGPS sources may be readily identified with SIMBAD objects with only limited rate of false coincidence (see e.g. Motch et al. 1991, Voges 1992). The second step consisted in selecting potentially interesting objects for optical identification at the telescope. Using the observational RASS X-ray properties of identified classes of X-ray sources together with other available information at a different wavelength such as the Guide Star Catalogue of the Hubble Space Telescope (Lasker et al. 1990) we could extract small subsets of sources having a higher probability to be identified with a given kind of X-ray emitter than in the overall survey installment. This approach led to several interesting results such as the discovery of a luminous supersoft source in the Galaxy (Motch, Hasinger & Pietsch 1994) and of a new class of X-ray soft intermediate polars (Haberl et al. 1994, Haberl & Motch 1995). The third step was the selection of several areas located

in particular directions of the Galaxy. Systematic optical identification of RGPS sources in these small sized regions allows to estimate at least statistically the X-ray content of the Milky Way as seen by ROSAT.

Several groups working in both hemispheres participate into the optical identification project in collaboration with scientists at the Max-Planck-Institut für Extraterrestrische Physik. We report here on the efforts carried out by one of the optical groups to optically identify ROSAT survey sources in a field located in the galactic plane. In this paper we present the details of the identification strategy and discuss the statistical properties of the sample which are likely to be representative of the overall properties of the galactic ROSAT X-ray sky. We also report on a few particularly interesting objects discovered in this field. The observed X-ray population of active coronae is compared with that predicted by stellar population models having resolution in age, folded with the most recent X-ray luminosity functions and the applications of such studies are shortly reviewed. We also put constraints on the contribution to the galactic plane X-ray emission of an hypothetical population of old neutron stars accreting from the interstellar medium. Observational details and source finding charts are presented in a companion paper (Motch et al. 1996a).

2. The Cygnus area

2.1. Selection from the ROSAT all-sky survey

The main scientific goal justifying the selection of this particular area in Cygnus was the study of the X-ray source population at very low galactic latitudes. At the time the optical observations started (1991 May) the Standard Analysis Software System (SASS; Voges et al. 1992) had analyzed a limited fraction of the all-sky survey. The only low galactic latitude areas then available were comprised between ecliptic longitude $\lambda = 343^\circ$ and $\lambda = 353^\circ$. Two years later, a larger field embracing the former one was interactively analyzed using the Extended Scientific Analysis System (EXSAS) developed at MPE (Zimmermann et al. 1992).

As a result of this two step X-ray reduction process the completeness of the optical investigations carried out in these two regions is slightly different and we shall define an 'inner' area corresponding to the part in which the first automatic analysis took place and a 'full' area corresponding to the EXSAS analysis.

Another complication arises from the existence of intense diffuse emission from the northern part of the Cygnus super bubble (see Fig. 1). The high number of spurious point-like sources produced by both the SASS and EXSAS analysis in regions of enhanced background and the resulting reduced sensitivity for detecting point sources led us to discard these specific areas amounting to a total of 13.5 deg^2 .

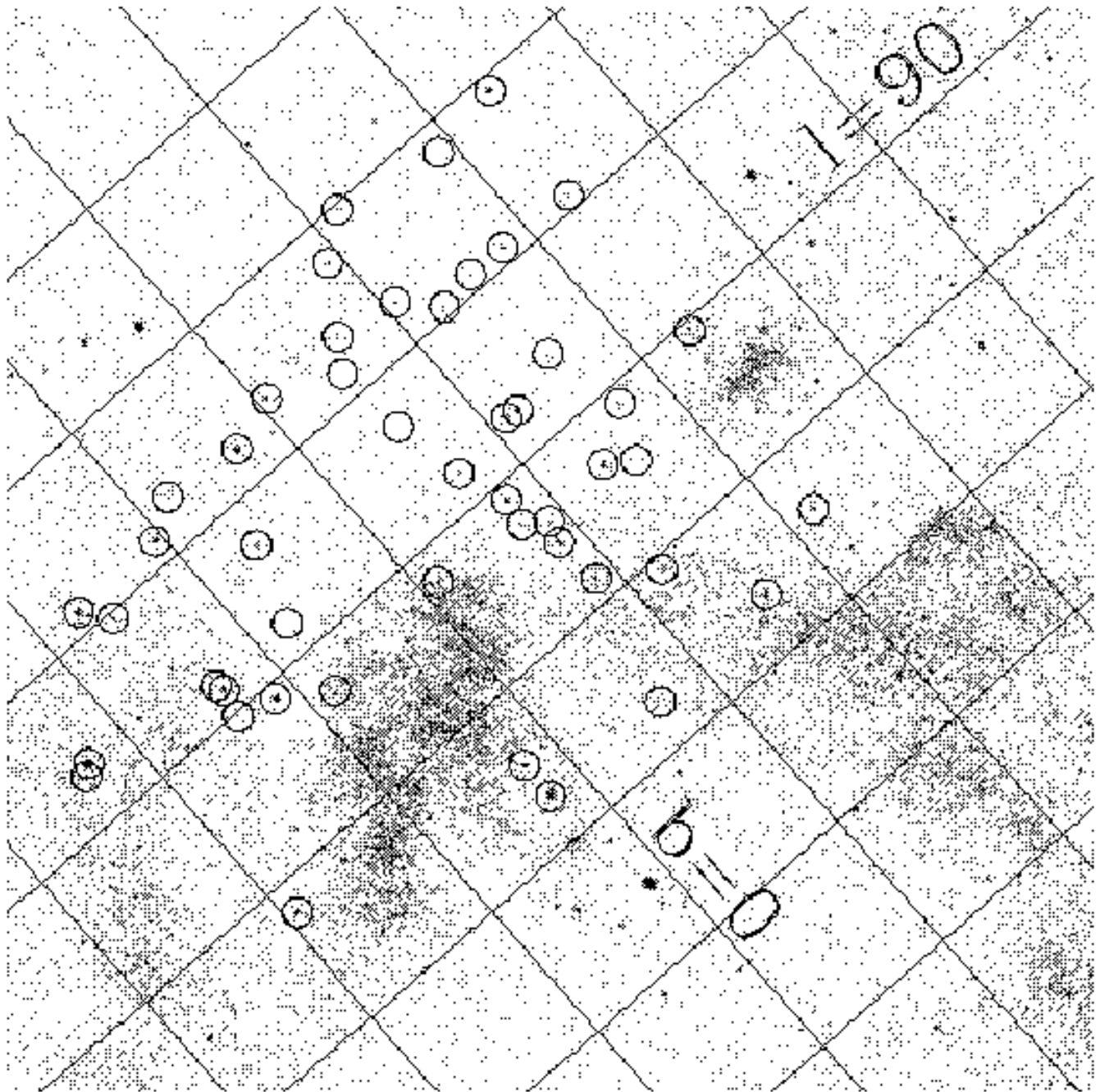


Fig. 1. ROSAT all-sky survey image of the Cygnus sample region (0.5-2.0 keV). The area is centered on $l = 90^\circ$ $b = 0^\circ$. The spacing of the coordinates grid is 2° . Intense diffuse emission from the northern part of the Cygnus X-ray super bubble is clearly seen. These notches of enhanced X-ray background were excluded from the final region which totals 64.5 deg^2 . Open circles mark the position of the point sources detected by the EXSAS interactive analysis. Few very soft sources are not visible in the hard image. For clarity we only show here sources with count rate larger than 0.03 cts s^{-1}

Both the 'inner' and 'full' areas are roughly centered at $l = 90^\circ$ and $b = 0^\circ$. The SASS analysis estimates the background from data collected within 4° wide strips parallel to the scan direction of the satellite in survey mode, whereas the interactive analysis allows to handle in one run all X-ray photons detected from the entire selected sky region. This difference of approach means that the source parameters, in particular, count rates, derived from the interactive run are in principle more reliable than those given by the automatic process and we shall not consider the latter in this paper. Also, a slightly lower source acceptance maximum likelihood (ML) for the 'full' area yielded the detection of several more sources in the 'inner' area.

The main features of the 'inner' and 'full' areas are listed in Table 1. We show on Figs 2 and 3 the positions of these two areas.

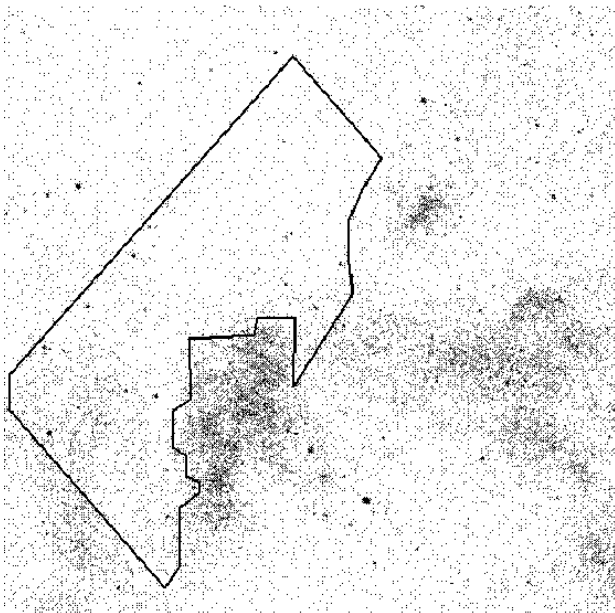


Fig. 2. The 'inner' area over-plotted on the ROSAT all-sky survey image (0.5-2.0 keV). The orientation is the same as in Fig. 1

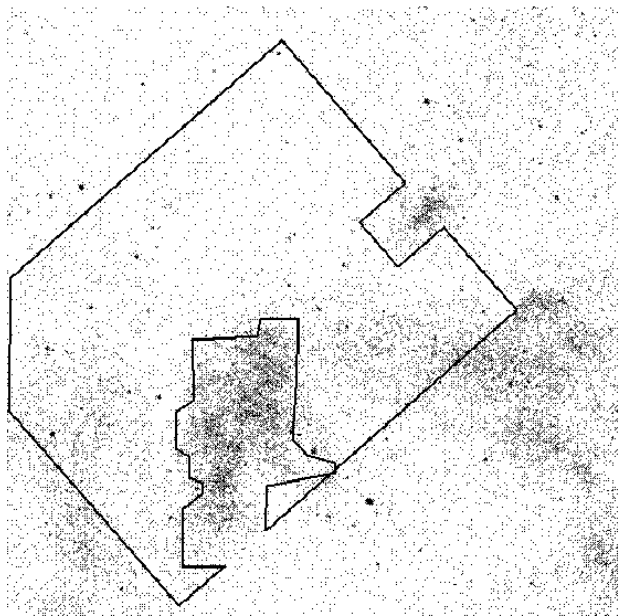


Fig. 3. The 'full' area over-plotted on the ROSAT all-sky survey image (0.5-2.0 keV). The orientation is the same as in Fig. 1

The selected area is located in a range of galactic longitude which is closest to the north ecliptic pole. Near the ecliptic poles the exposure time in the ROSAT all-sky survey reached the maximum and therefore a strong gradient in exposure time is present in the selected field from about 500 s at $b = -5^\circ$ to 1000 s at $b = 5^\circ$. However, our sample is rather homogeneous since 84% of the sources have exposure times ranging from 700 to 900 s. Other areas in the galactic plane have lower exposures, like e.g. the galactic center region with only a few hundred seconds (see the exposure map of the ROSAT all-sky survey in Snowden et al. 1995).

The background level in the PSPC image, determined from source-free areas outside the diffuse emission regions shows no strong variations and was between 0.7 and 0.8 counts per square arcmin for the full energy band of 0.1 - 2 keV. The source detection using the maximum likelihood technique from the EXSAS package was done in three energy bands, namely 0.1 - 0.4 keV, 0.5 - 2.0 keV and 0.1 - 2.0 keV. Sources were formally accepted above a maximum likelihood value of 7. Because of the high expected level of spurious sources among the very low ML detections (up to 0.29 sources per square degree or ≈ 19 spurious detections with $ML \geq 7$ over the 'full' area, see section 9.3) we only considered sources with $ML \geq 8$ for most statistical purposes. Each of these sources, listed in Table 11, has an associated running index ranging from 1 to 128 and increasing with decreasing count rates. Since some of the detections with ML between 7 and 8 had established optical counterparts of scientific interest, we sep-

Table 1. Characteristics of the investigated areas

	'inner'	'full'
Area (deg ²)	38.1	64.5
Number of sources		
ML ≥ 7	106	158
ML ≥ 8	88	128
ML ≥ 10	67	95

arately listed in Table 12 these additional sources which were given index numbers in the range of 129 to 158.

The area analyzed here is about 1/4 of that covered by the whole Einstein Galactic Plane Survey (Hertz & Grindlay 1984, 1988). However, the flux completeness level of our sample in Cygnus is ≈ 4 times fainter and accordingly the total amount of sources studied in this paper is comparable to that in the total Einstein survey.

2.2. Astrophysical characteristics

In the direction of $l = 90^\circ$, $b = 0^\circ$, the line of sight first crosses the local spiral arm during the first 1 kpc and then reaches the Perseus arm at a distance of about 4 kpc (e.g., Vogt & Moffat 1975, Georgelin & Georgelin 1976). Further away, the HI Cygnus arm (Kulkarni et al. 1982) is encountered at a distance of ≈ 11 kpc.

Two molecular cloud systems dominate the interstellar absorption and are well visible on Fig. 4. At $l \leq 87^\circ$ the edge of the Cygnus Rift cloud complex appears. However, the main structure is the cloud related to the CYG OB7 association (Dame & Thaddeus 1985) located in the $l \geq 90^\circ$; $b \geq 0^\circ$ part of our selected region. From CO measurements Dame & Thaddeus (1985) derive distances of 700 - 800 pc for these two molecular clouds, well within the local spiral arm. These two structures are also visible in the optical absorption map of Neckel & Klare (1980) at a comparable distance. Finally, a similar structure may be seen in the dark cloud map of Feitzinger & Stüwe (1986).

Our sample region overlaps with the north-east part of the X-ray super-bubble discovered by Cash et al. (1980). This ring-shaped soft X-ray diffuse emission is well seen in Snowden et al. (1995). This hot bubble is thought to be located at a distance of about 2 kpc and its total angular extent of 13° implies a diameter of 450 pc. The total X-ray energy radiated is $5 \cdot 10^{36} \text{ erg s}^{-1}$ at a temperature of $2 \cdot 10^6 \text{ K}$ and the total energy content of the bubble is estimated to be of the order of 10^{51} ergs (Cash et al. 1980). The origin of this large structure is unknown but probably related to the Cyg OB2 association. A series of 30-100 supernovae during the last 3-10 million years or hot winds emanating from OB associations and interacting with the interstellar medium could explain the X-ray emission.

3. Optical identification procedure

3.1. SIMBAD identifications

Our first step toward optical identification was to search the SIMBAD database for positional coincidence with a catalogued object. For the entire galactic plane survey, about 20% to 30% of the sources may be readily identified with SIMBAD entries with an expected number of random spurious coincidence of about 10% of the identifications (Motch 1992). A similar identification rate was derived from the analysis of a small area in the galactic plane in Perseus (Motch et al. 1991).

In our 'full' area, 30 among 95 sources (i.e. 31%) detected at a maximum likelihood larger than 10 have SIMBAD entries within r_{90} the 90% ROSAT survey confidence radius. Scanning the database shows that the mean density of SIMBAD objects in a $10^\circ \times 10^\circ$ region centered on $l = 90^\circ$, $b = 0^\circ$ is ≈ 130 per square degree. With an average $r_{90} = 25''$ ($ML \geq 10$), we expect a random match in $\approx 2\%$ of the cases. This lower false identification rate compared to former studies is due to the improved accuracy of survey X-ray sources positioning with respect to the first analysis. We thus expect 2 wrong identifications among the 30 SIMBAD proposed matches. However, the spatial density of SIMBAD entries may be locally much higher because of the inclusion of a particular catalogue (e.g. the catalogue of objects in the direction of M39 compiled by Platais, 1994). Therefore, whenever the information retrieved from the literature was not firmly conclusive we tried to obtain our own optical data.

3.2. Optical observations

All optical data were obtained at the Observatoire de Haute-Provence in the time interval from 1991 May till 1993 September. A description of the instrumentation used may be found in Motch et al. (1996a).

For each ROSAT source we produced a finding chart using the HST Guide Star Catalogue (GSC, Lasker et al. 1990). GSC data were extracted in a first step from the STARCAT facility at ESO (Pirenne et al. 1993) and later from the SIMBAD catalogue GSC browser (Preite-Martinez & Ochsenbein 1993).

In the cases where one or more rather bright GSC stars were lying close to the center of the X-ray position, with apparently a rather low probability of random coincidence, we directly started our investigation by obtaining medium resolution spectroscopy ($\lambda\lambda$ 3800 - 4300 Å; FWHM resolution $\approx 1.8 \text{ Å}$) of the GSC candidates. These spectra allowed the detection of re-emission in the Ca II H&K lines which is a well known signature of chromospheric and associated coronal activity (e.g. Schrijver 1983, Maggio et al. 1987). When the chromospheric activity was not found at the level expected from the intensity of the X-ray source (see below) or when no bright GSC star was conspicuous in the error circle, we obtained B and I band CCD photometry of the field. From the B-I index we could select stars exhibiting a red excess, presumably dM star candidates and blue excess objects considered as candidates for white dwarfs, cataclysmic variables and background AGNs. We then obtained low resolution spectroscopy ($\lambda\lambda$ 3500 - 7500 Å; FWHM resolution $\approx 14 \text{ Å}$) of the photometric candidates and of other faint sources if necessary. We tried to push our optical low resolution spectroscopic investigations at the same limiting magnitude for all sources at a given X-ray count rate in order to preserve as much as possible the completeness of the identified sample. This means that for the X-ray brightest unidentified sources

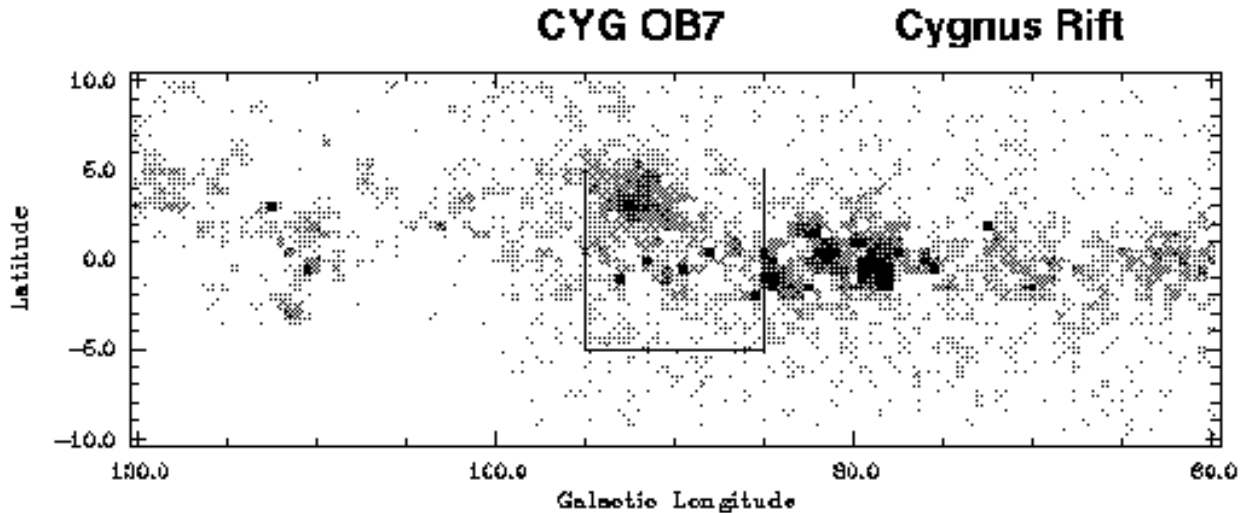


Fig. 4. CO map (after Dame et al. 1987) of the galactic plane in a region surrounding our ROSAT survey sample area. The square shows the approximate location of the area studied in X-ray. In this region the dominant structure is the CYG OB7 molecular cloud. A small part of the Cygnus Rift is also visible. These two complexes are located at ≈ 700 -800 pc. The peak of emission at $l = 80^\circ$ is Cygnus X

we are complete down to $V \approx 17$ -18. However, considering the sometimes relatively high number of objects encountered in the error circles and the changing instrumental conditions our optical depth is probably not quite homogeneous.

4. Optical identifications

4.1. Extragalactic sources

Active galactic nuclei account for almost 70% of all extragalactic identifications in the Einstein Extended Medium Sensitivity Survey (EMSS; Stocke et al. 1991) which has a median sensitivity close to that of the ROSAT all-sky survey. With this X-ray sensitivity AGNs have reddening free V magnitudes in the range of 14 to 20 (Gioia et al. 1984). Redshifted broad and narrow emission lines are easily recognizable optical signatures even at low signal to noise ratio. From HI and CO data we find that the clearest part of the 'full' region has only $A_V \approx 2$ -3 mag whereas the most absorbed part has $A_V \geq 15$ mag. Therefore we do not expect to identify many AGNs with our instrumental spectroscopic limit of $V \approx 18$ and may consider our only identified AGN at $V = 16.3$ as outstanding. The situation is even more unfavourable for clusters of galaxies

which constitute the second most numerous class of extragalactic sources. Their intrinsic optical faintness and the high galactic stellar foreground make their recognition on a CCD image almost impossible in such a low latitude region. Finally the lack of marked optical signatures renders identification of BL Lac objects probably hopeless.

4.2. White dwarfs

Because of the very pronounced effect of interstellar absorption on their intrinsically very soft X-ray spectra, most of the white dwarfs detected by ROSAT undergo very little interstellar absorption and thus appear basically unreddened at optical wavelength. The hottest DA and DO members which are the most likely to be serendipitously discovered by ROSAT exhibit only weak and shallow H or He absorption lines (Wesemael et al. 1993) which are sometimes difficult to detect for the optically faintest objects. Therefore, we rather considered the very blue Rayleigh-Jeans like continuum as the definite signature of a white dwarf. Of the three white dwarfs detected in our sample area one was already catalogued as such (GD 394). The optically brightest of the two new white dwarfs was found recently in a list of UV excess objects in the galactic plane (LAN 121; Lanning & Meakes 1994).

4.3. Early type Stars

Einstein X-ray observations have shown that early type stars may have soft X-ray luminosities as large as a few 10^{33} erg s $^{-1}$. Pallavicini et al. (1981) demonstrated that the soft X-ray and bolometric luminosities of O-B stars were tightly correlated with $L_X \approx 10^{-7} L_{\text{bol}}$. Among the ≈ 300 stars earlier than B5 listed in SIMBAD for our Cygnus survey area, we detect two of the three optically brightest ($B \leq 6.0$) (HR 8154, $B = 4.99$, O8e and HD200310, $B = 5.16$, B1Ve) but we miss the overall brightest one (HR 8047, $B = 4.69$, B1.5nne). These stars have photometric distances of the order of 600 pc and are probably members of the CYG OB7 association. In these two cases, the X-ray luminosities are consistent with normal coronal emission from the OB star. Our third detection is HR 8106 which is a B9III/Ap star rather than a hot early type star and the inferred X-ray luminosity ($L_X \approx 1 \cdot 10^{30}$ erg s $^{-1}$) is consistent with that of a late type active companion star.

4.4. Active coronae

The fact that many late type stars were bright soft X-ray sources was one of the important discoveries of the Einstein observatory (Vaiana et al. 1981). X-ray coronal activity is now known to be a common feature of many stars of spectral type later than about A5 (e.g. Rosner et al. 1985 and references therein). Observed stellar X-ray luminosities are in the range of 10^{26} - 10^{31} erg s $^{-1}$. They increase with rotation rate (Pallavicini et al. 1981) and decrease with stellar age (Micela et al. 1988), pre main sequence stars being about 1000 times more luminous than old main sequence objects. Although a satisfactory theory accounting for all aspects of stellar X-ray activity is not yet available, the currently accepted picture is that X-ray emission originates from a hot stellar corona. By analogy with what is known from the Sun the bulk of X-ray emission is thought to come from magnetically confined loop-like structures emerging at the stellar surface and which are likely to be generated in the subphotospheric convective layers by a dynamo mechanism.

Unfortunately, there is no bright spectral signature of coronal activity at optical wavelength. However, chromospheric and coronal activities are known to be well correlated in the Sun and late type stars in general (see e.g. Reimers 1989 and references therein). In particular, the Ca II H&K chromospheric emission lines are very sensitive measurements of stellar activity which behaves like X-ray emission in being more intense in fast rotating and young stars (Wilson 1963, 1966). Studies based on Einstein X-ray data have shown that the strength of these emissions is indeed well correlated with X-ray luminosity (e.g. Schrijver 1983, Maggio et al. 1987, Fleming et al. 1988).

4.4.1. Optical spectroscopy

Using medium resolution blue optical spectra of ≈ 100 stars associated with RGPS sources Guillout (1996) has established and calibrated the relation between Ca II H&K and PSPC flux. Basically, Ca II H&K and soft X-ray emissions are found to be correlated both in flux and luminosity with $F_{\text{CaII}} \sim F_X^{0.74 \pm 0.14}$ and $L_{\text{CaII}} \sim L_X^{1.05 \pm 0.20}$. These relations hold over 2 decades in flux and over 3 decades in luminosity. The existence of a flux/flux correlation leaves no doubt that the luminosity relation is real and not an artifact of the distribution in distance. A rms scatter of about a factor 2 in flux / luminosity exists around the mean trend with a maximum range of a factor 10. This scatter is probably caused by the long term (solar cycles) and short term (flares) variability of the coronal/chromospheric activity since our spectroscopic measurements were obtained on the average 2 years after the X-ray survey observations. In spite of this dispersion the above relations may still be extremely valuable tools for identifying active coronae.

The distances in the $\log(L_{\text{CaII}}) / \log(L_X)$ diagram between the position of each active corona and the mean relation have an apparently Gaussian distribution with $\sigma = 0.30$ (Guillout 1996). We show in Fig. 5 the distribution of these distances for our sample in Cygnus. In order to quantify the Ca II identification criterion we computed for each star P_{CaII} , the formal probability that if the star is responsible for the X-ray emission its chromospheric emission appears fainter or equal to the observed value.

Several M stars which were optically too faint for medium resolution spectroscopy were observed at low resolution ($\lambda\lambda$ 3500- 7500 Å; FWHM resolution ≈ 14 Å). In these cases, we considered that the detection of Balmer emission unambiguously identifies the X-ray source with the late type star. It is known that active M dwarfs tend to have stronger Balmer over Ca II H&K emission ratios than earlier types (Rutten et al. 1989) and that H α and X-ray emissions tightly correlate (Fleming et al. 1988). In order to check the validity of our Me star identifications we computed H α fluxes using our spectra and the V magnitudes extracted from the literature or from our own measurements. X-ray luminosities were estimated assuming $F_X \approx 10^{-11} \times S$ erg cm $^{-2}$ s $^{-1}$ where S is the PSPC count rate in cts s $^{-1}$. For RX J2104.1+4912 (index 7) we used the quiescent X-ray count rate (see sect. 6). In the $L_X / L_{\text{H}\alpha}$ diagram (Fig. 6) our Me stars occupy a region similar to that occupied by the Me stars identified in the EMSS (Fleming et al. 1988) or by Skumanich et al. (1984). Considering the remaining photometric errors of ≈ 0.3 mag and keeping in mind the slightly different X-ray energy ranges between ROSAT and Einstein we consider that the agreement is good and leaves no doubt that we have correctly identified these X-ray sources.

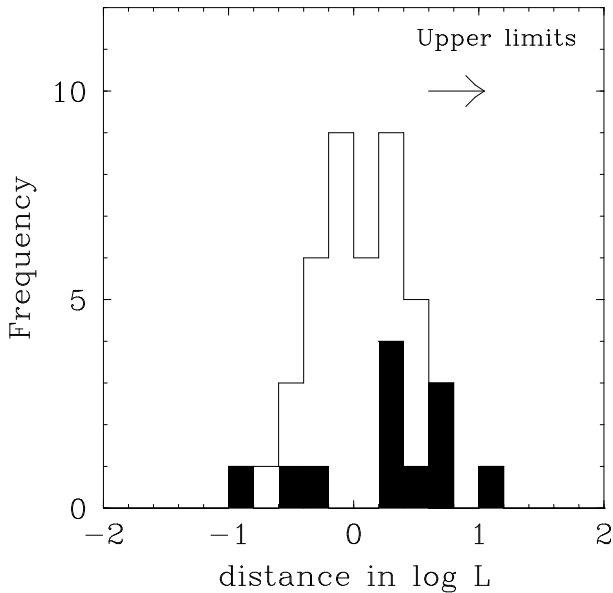


Fig. 5. Histogramme of the distance to the best $\log(L_{\text{CaII}}) / \log(L_X)$ relation for 44 candidate stars in Cygnus (measured values and upper limits). The filled histogram represents stars for which only an upper limit on CaII H&K emission is available. Stars with positive log distances exhibit less CaII emission with respect to their X-ray flux than for the average identified sample and on this basis may be considered as less likely counterparts

4.4.2. Positional coincidence with GSC

Visual examination of our Guide Star Catalogue finding charts readily showed that in many cases the X-ray position was quite close to a rather bright (typically $V \leq 12$) star usually unreferenced in SIMBAD. In order to obtain an additional identification criterion we computed the a priori probability of positional coincidence by systematically scanning the GSC catalogue within $20'$ from the ROSAT position. Care was taken to remove duplicate stars in the regions of plate overlaps. We show on Fig. 7 the density of GSC entries held in a ring-shaped area centered on the X-ray position as a function of the radius. The high density excess of stars close to the X-ray position shows that a sizeable fraction of our X-ray sources have indeed counterparts in the GSC catalogue. For instance, 59 GSC entries are found within $30''$ from the X-ray position whereas the expected number of random matches is only 4. This example shows that in the galactic plane at least, systematic cross-correlation of the ROSAT all-sky survey sources with GSC entries should allow efficient source selection if not identification.

For each X-ray position with a GSC entry of magnitude V within r_{90} we defined the a priori probability of a spurious match within r_{90} as $P_{\text{spurious}} = N_V \times \left(\frac{r_{90}}{20'}\right)^2$ where

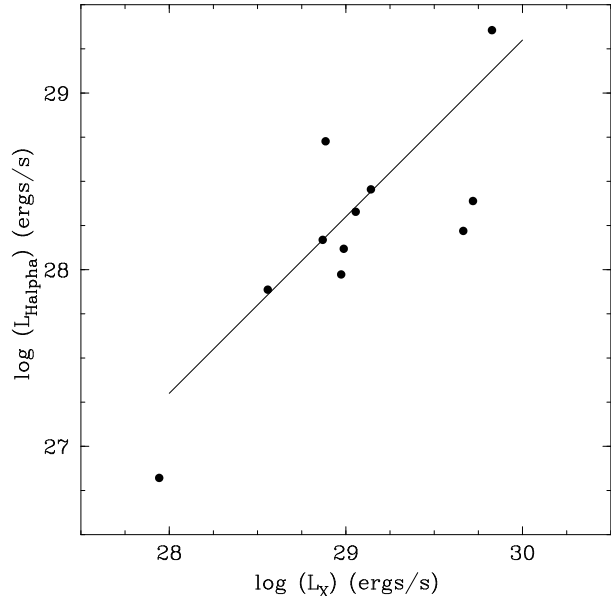


Fig. 6. Comparison of chromospheric $H\alpha$ and coronal X-ray luminosities for 11 Me stars identified in the 'full' area and having a low resolution spectrum. The solid line represents the relation found by Skumanich et al. (1984) which is also representative of the EMSS Me stars

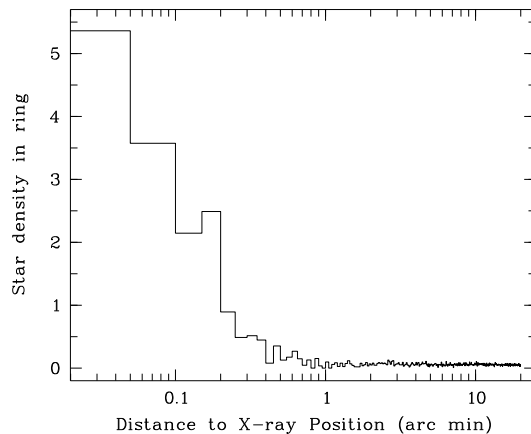


Fig. 7. Mean density of GSC entries (arcmin^{-2}) in a ring of $3''$ width centered on the X-ray position as a function of the radius of the ring. The density shown here is the average for 95 sources of the 'full' area having a maximum likelihood larger than 10. The clear excess of matches at small distances demonstrates the possibility to automatically identify sources with GSC entries (or at least select active coronae candidates)

N_V is the number of GSC entries of magnitude brighter or equal to V found within $20'$ from the ROSAT source. In a similar fashion we define the a priori probability of identification of the X-ray source with the GSC star as $P_{\text{GSC}} = 1 - P_{\text{spurious}}$. When no GSC entry was found within r_{90} we set $P_{\text{GSC}} = 0.0$ and used the CaII H&K emission alone as identification criterion.

We show in Fig. 8 the histograms of P_{spurious} for the samples of candidate stars having a CaII measurement compatible with the X-ray emission (i.e. with a probability of more than 2% to belong to the mean CaII / X luminosity relation) and for those proposed on the only basis of their proximity to the X-ray position. The two distributions look alike and by integrating the probabilities one expects in total 0.6 among 35 and 1.7 among 53 false cases in the spectroscopic and positional selected samples respectively. This gives us confidence in the possibility to identify X-ray sources with rather bright GSC entries, all presumably active coronae, without obtaining time consuming medium resolution spectroscopy.

Because of the late interactive re-analysis of X-ray survey data in this field, we could spend significantly more observing time per source in the 'inner' area than in the 'full' area. Consequently, the majority of our spectroscopic sample is in the 'inner' area. For the sources located outside the 'inner' area, we concentrated on X-ray locations without bright GSC candidates relying on the probability of positional coincidence to identify the un-investigated X-ray sources.

Note that for convenience we arbitrarily assigned a position probability of 1.0 to our optical identifications with AGN, white dwarfs and Me and late Ke stars. A couple of stars with GSC positions inside r_{90} (sources index 13 and 80) were eventually found slightly outside when using SIMBAD coordinates.

4.4.3. Combined identification criteria

The positional and CaII probabilities have different natures since we are dealing on one hand with the probability that a bright unrelated star falls into the ROSAT error circle and on the other hand with the probability that a given star is actually related to the X-ray source once it is found close to the ROSAT position. As a rule of thumb we decided to set the probability boundaries such as the number of spurious or missed identifications among the considered samples was of the order of 1. Since in the 'full' area, we have 44 candidate active coronae with a GSC match and no spectroscopy available and the same number of candidate stars with spectroscopic observations, we decided to identify with active coronae all X-ray sources having either $P_{\text{GSC}} \geq 98\%$ or $P_{\text{CaII}} \geq 2\%$. Stars without measured CaII flux or with $P_{\text{CaII}} < 2\%$ and $95\% \leq P_{\text{GSC}} < 98\%$ were considered as potential optical counterparts and marked with a '?' in columns 'Class' and 'Identification' of Table 11 and 12. We count 13 such 95% confidence

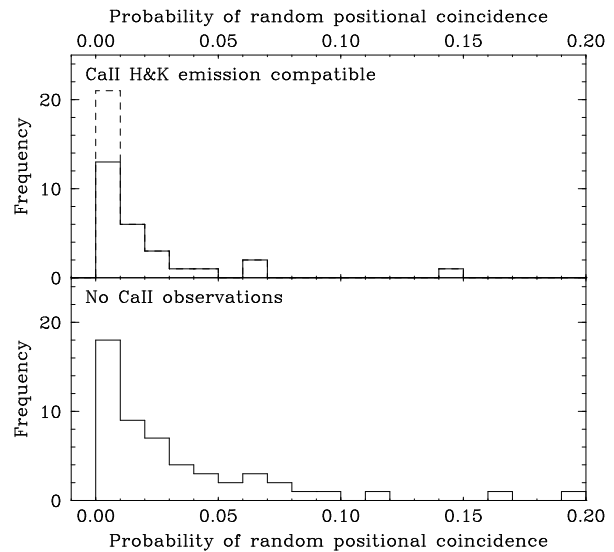


Fig. 8. Histogramme of the probabilities of random positional coincidence of X-ray sources with GSC entries. Upper panel: all stars having a measured CaII H&K emission compatible with ROSAT X-ray flux, solid line; only detection, dashed line; including compatible upper limits. Lower panel: proposed candidate stars without spectroscopic observations. The two distributions are similar and the expected total number of false coincidence is 0.6 among 35 for the spectroscopic sample and 1.7 among 53 for the positional sample. This demonstrates that in the galactic plane one may identify ROSAT survey sources with GSC entries with a high success rate on the basis of positional coincidence only

level identifications with $ML \geq 8$ whereas only ≈ 4 such random associations are expected for a set of 128 sources. This illustrates further the usefulness of the Guide Star Catalogue for identifying RASS sources at low galactic latitudes.

We list in Table 2 the statistics of the origin of identifications with active coronae for the original 'inner' and 'full' areas. The distribution in count rates of the two identified samples is shown in Fig. 9.

Table 2. Origin of active coronae identifications for sources with maximum likelihood larger than 8

Criterion of identification	'inner'	'full'
CaII H&K emission ($P_{\text{CaII}} \geq 2\%$)	32	40
Low resolution spectroscopy	8	9
Positional coincidence only ($P_{\text{GSC}} \geq 98\%$)	16	25
Total number of identified active coronae	56	74

Among the 44 candidate stars located in the 'full' area and having medium resolution spectra, we find 4 cases (all upper limits) where the probability that the observed CaII

emission is compatible with X-ray emission is smaller than 2% whereas the normal distribution would predict only one such case. For two of these sources (RX J2055.3+5025, index 15 and RX J2054.1+4942, index 44) the optical counterpart is bright ($V \leq 11$) and the a priori chance probability of positional random coincidence derived from the GSC surroundings is correspondingly very small, typically less than 1%. These two bright candidates of spectral types F8 and G0 have strong photospheric Ca II flux and any emission will have lower contrast than in later type stars. Velocity differences between emission and absorption components produced by fast rotation or binarity will further decrease the Ca II contrast. In the two remaining cases (RX J2132.5+4849, index 51 and RX J2054.6+5120, index 72), the probability of random coincidence is much larger ($\geq 5\%$) and we shall not consider these two identifications. All 8 stars for which we only had Ca II upper limits compatible with the observed ROSAT X-ray flux also had $P_{\text{GSC}} \geq 98\%$ and on this basis were considered as reliable optical identifications.

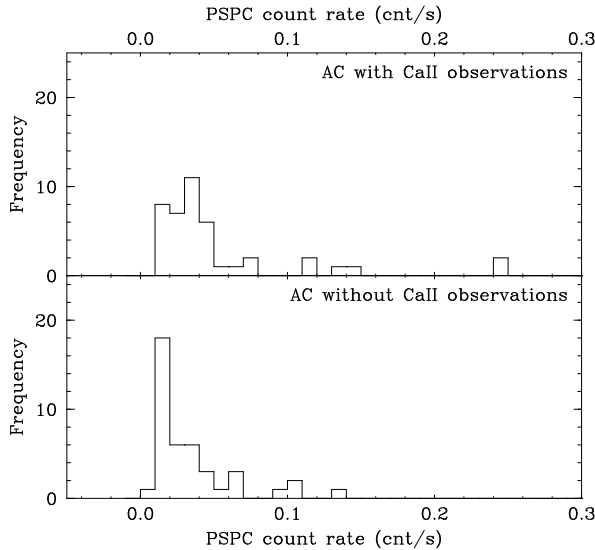


Fig. 9. Histogramme of the PSPC count rates for active coronae identified in the ‘full’ area on the basis of the strength of their Ca II H& K emission (upper panel) and on the basis of positional coincidence only (lower panel). The difference of the source distribution reflects our optical identification strategy

5. Overall source statistics

5.1. Completeness of identification and repartition by types

The final list of proposed optical counterparts including the positional and Ca II derived probabilities of identification are listed in Tables 11 and 12. We show in Tables

3 and 4 the statistics of source identifications in the ‘full’ area for several limiting count rates. For sources detected with $ML \geq 10$, the X-ray completeness level is $\approx 0.02 \text{ cts s}^{-1}$ (see section 9) and at this limit we have optically identified 88% of the sources. Active coronae constitute the overwhelming majority of our sample. The contribution of white dwarfs reduces the stellar fraction at high count rates and the incompleteness of the optical identification again decreases the fraction of active coronae at low count rates. At the level of $0.03\text{--}0.025 \text{ cts s}^{-1}$ which is about the median all-sky survey sensitivity we have identified over 95% of the sources and active coronae account for about 85% of the total population in our low galactic latitude field. A high fraction of active coronae was also found in the Einstein Galactic Plane Survey ($\approx 46\%$; Hertz & Grindlay 1984, 1988) and in a ROSAT sample area in Perseus ($\approx 48\%$; Motch et al. 1991). Our record beating percentage of active coronae in Cygnus obviously reflects the location at $b = 0^\circ$ of our area. A similar test region in the Taurus Constellation, away from the main star forming region ($b \approx -14^\circ$; $l \approx 180^\circ$) also contains $\approx 77\%$ of active stars with an optically identified extragalactic population of $\approx 13\%$ (Guillout 1996). At higher galactic latitudes, the fraction of active coronae identified in the RASS falls to $\approx 42\%$ (Zickgraf et al. 1996) and may reach values as low as 10% at the north galactic pole (Zickgraf 1996). It is thus amazing that in spite of the apparently nearly constant density of ROSAT survey sources with galactic latitude ($\approx 1.5 \text{ deg}^{-2}$; Voges 1992) their nature changes from an extragalactic dominated to star dominated population while moving to lower galactic latitudes.

Table 4. Source identification statistics in the ‘full’ area. Figures are in percents

Limiting Count rate	Fraction of Active Coronae	Fraction Identified
0.1	67	100
0.05	81	100
0.03	85	98
0.025	84	95
0.02	79	88
0.015	68	75
0.01	56	62

5.2. Positions and 90% confidence radii

An accurate knowledge of the ROSAT error circle is of utmost importance for guiding the optical observations in the crowded fields often encountered at low galactic latitude. An illustrative example is probably our discovery of the WD+Me binary RX J2130.3+4709 (index 84). Spectroscopy of the bright ($V = 8.45$) G0V star HD 204906

Table 3. Source identification statistics in the 'full' area (all ML). Figures are number of sources

Limiting count rate	Total number of sources	Active coronae	OB	AGN	CV or related	White dwarfs	Unidentified
0.1	12	8	-	1	-	3	-
0.05	21	17	-	1	-	3	-
0.03	48	41	2	1	-	3	1
0.025	57	48	2	1	-	3	3
0.02	68	54	2	1	-	3	8
0.015	101	69	2	1	1	3	25
0.01	138	77	3	1	2	3	52

failed to reveal convincing Ca II emission and furthermore the star was clearly outside the r_{90} radius. This led us to investigate other candidate stars closer to the X-ray position and discover this interesting system.

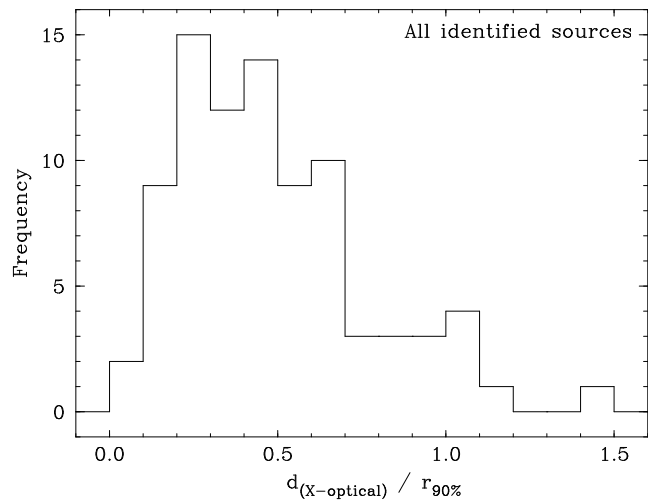
The errors on ROSAT X-ray positions have two different origins. First, the uncertainty with which the centroid of the X-ray image is positioned on the pixel grid by the maximum likelihood source detection algorithm. Second the error in the knowledge of the satellite attitude for each photon collected in scan mode. Early analysis led to the conclusion that the error on the position was dominated by the ROSAT attitude bore sight accuracy and that assuming a Gaussian two-dimensional distribution the final uncertainty could be written as:

$$r_{90} = 2.15 \times \sqrt{\Delta_{xy}^2 + \Delta_{att}^2}$$

where Δ_{xy} is the maximum likelihood error and where Δ_{att} , the attitude uncertainty was estimated to be $\approx 8''$ from a subset of X-ray binaries with accurate positions (Motch et al. 1996b). Applying this estimate to the sources in our survey field yields a mean r_{90} in the range of $19''$ to $32''$ slightly depending on the maximum likelihood of detection (see Table 5). The histogram of the distance between X-ray and optical positions expressed in units of the 90% confidence radius (see Fig. 10) is compatible with a normal Rayleigh distribution. The fact that only $\approx 7\%$ of all 86 proposed optical counterparts are located outside r_{90} from the ROSAT position suggests that we may have slightly overestimated the satellite attitude error and that the actual Δ_{att} is close to $7''$. Adding the 14 less secure candidates identified at the 95% confidence level only does not change this conclusion. However, the identification strategy may have favoured optical counterparts located close to the X-ray position. The positions extracted from SIMBAD are based on 1950 coordinates and are not corrected for proper motion. Also the "Quick V" plate collection on which are based the northern GSC coordinates was obtained in the 1982-1984 interval and these positions may be altered to some extent by the unknown proper motion. Therefore, a small fraction of the scatter in the distance between X-ray and optical positions may be due the lack of correction for proper motion.

Table 5. 90% confidence radii for various maximum likelihood

Maximum likelihood of detection	Mean $r_{90}('')$	Mean Count rate (cts s ⁻¹)
≥ 100	19.2	0.300
50 - 100	22.4	0.066
20 - 50	23.8	0.035
10 - 20	28.8	0.019
≤ 10	32.3	0.012

**Fig. 10.** Histogramme of the distances between X-ray and optical positions expressed in units of the computed 90% confidence radius. The distribution is shown here for the 86 sources identified in the Cygnus area

5.3. X-ray hardness ratios

In principle hardness ratios are powerful tools to select and guide the identification of ROSAT X-ray sources (see e.g. Motch 1992). However, the use of X-ray colours is essentially limited to the brightest sources. With a mean exposure time of the order of 800 s useful information may be extracted for the sources having count rates larger than ≈ 0.02 cts s⁻¹. We show in Fig. 11 the distribution of a subset of 62 sources with count rates larger than 0.012 cts

s^{-1} , in the HR1/ HR2 diagram. Hardness ratios 1 and 2 have here energy boundaries as used in the latest SASS versions:

$$HR1 = \frac{(0.5 - 2.0) - (0.1 - 0.4)}{(0.1 - 0.4) + (0.5 - 2.0)}$$

$$HR2 = \frac{(1.0 - 2.0) - (0.5 - 1.0)}{(1.0 - 2.0)}$$

where (A-B) is the raw background corrected source count rate in the A-B energy range expressed in keV. Identified active coronae span a wide range of X-ray colours consistent with the variety of temperatures encountered in stars (e.g. Schmitt et al. 1990). White dwarfs populate the soft region of the diagram while our only identified AGN exhibits the hard X-ray colours expected from a heavily absorbed source. The unidentified source RX J2133.3+4726 (index 35) is located on the sky close to the identified AGN and displays hard X-ray colours ($HR1 = 0.96 \pm 0.27$; $HR2 = 0.62 \pm 0.16$). Deep optical searches in this error circle indeed rule out identification with active coronae (Motch et al. 1996a). This suggests a remote luminous source possibly of extragalactic nature. The O8Ve star HR 8154 also exhibits a soft HR2 and hard HR1 which probably originates from a substantial interstellar absorption toward this remote ($d \approx 640$ pc) source in CYG OB7. Active coronae detected at large distance may have harder HR1 than closer ones (see Fig. 12). However, this effect could either be due to enhanced photoelectric absorption towards most distant objects and / or to intrinsically higher temperatures usually observed for the most luminous active coronae which are obviously the ones we detect at the largest distances (Schmitt et al. 1990).

5.4. X-ray variability

Owing to the snapshot nature of survey observations for which we have at best a 32 s long integration every 96 min only limited information on time variability is available. However, active coronae are known to exhibit large X-ray flares and one may wonder whether a sizeable fraction of our sources is detected thanks to these fast events. Visual inspection of the light curves produced in the broad (0.1-2.0 keV) and hard (0.5-2.0 keV) X-ray band reveals that most active coronae were detected during all satellite orbits and that the flaring activity is in general not prominent. Our only conspicuous flare originates from the Me star RX J2104.1+4912 (index 7; see Fig. 13). In the absence of this particular event, the mean count rate from the source would have been 0.062 cts s^{-1} instead of the 0.13 cts s^{-1} . Accordingly, we conclude that the effect of flares is not important in our sample and that there is no large bias in favour of the preferential detection of flare stars.

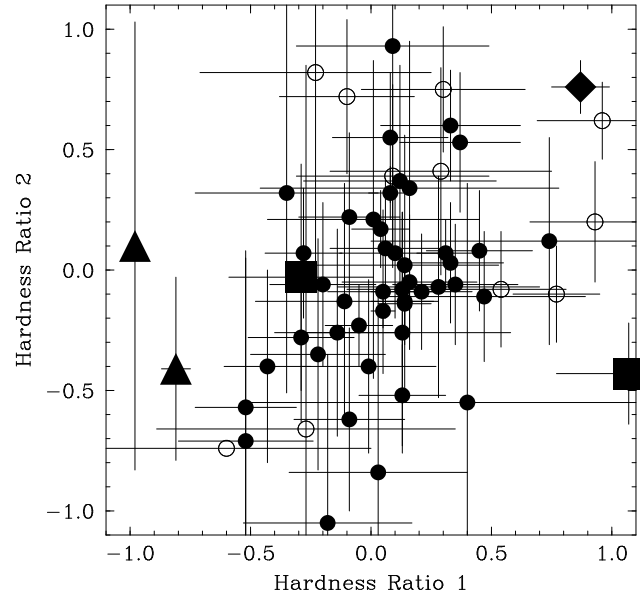


Fig. 11. Distribution of a subset of 62 sources having computed hardness ratios. Unidentified sources are represented as open circles. Identified active coronae (filled circle) populate the center of the diagram and span a rather large range in HR1 and HR2. White dwarfs (filled triangle) with soft HR1 clearly stand out of the dominant stellar population. The only optically identified AGN (filled diamond) is hard in both X-ray colours as a result of the large intervening photoelectric absorption. Of the two objects flagged as 'OB' stars (filled squares) one is a B9III/Ap candidate which displays X-ray colours similar to active coronae. The early type star HR 8154 exhibits very hard HR1 due to interstellar absorption and rather soft HR2 consistent with the emission of an O8Ve star at the distance of the OB association CYG OB7

6. Stellar population

As stated above, the population of active coronae dominates our sample and down to a flux level of 0.03 cts s^{-1} stars account for 85% of the total number of field sources. Unfortunately, we do not have spectra for all star candidates in the 'full' area. However, in the restricted 'inner' area (38.1 deg^2) we have spectroscopic information from the literature or from our own observations for all 42 identified X-ray stars detected above a count rate of 0.02 cts s^{-1} . We list in Table 6 the repartition in spectral type of this complete subsample.

It is known that single A stars are very weak X-ray emitters in agreement with their almost absent convective zone and chromospheric activity. Therefore our identification of a small fraction of X-ray sources with A stars, here only based on a very low probability of random coincidence, may only be understood if one assumes the presence of an X-ray active companion of lower mass. Considering the rather short main sequence life time of A stars (\leq

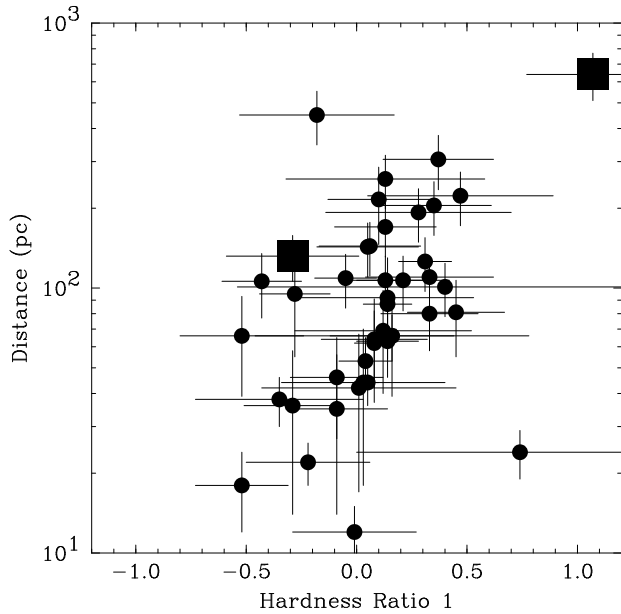


Fig. 12. Distribution in HR1 and distances for a subset of active coronae (filled circles) and OB and B9III/Ap stars (filled squares). Distant sources may display harder X-ray spectra than nearby ones. In the absence of detailed spectral fitting this effect could be either due to interstellar photoelectric absorption and / or to the higher temperatures usually observed in the most luminous active coronae

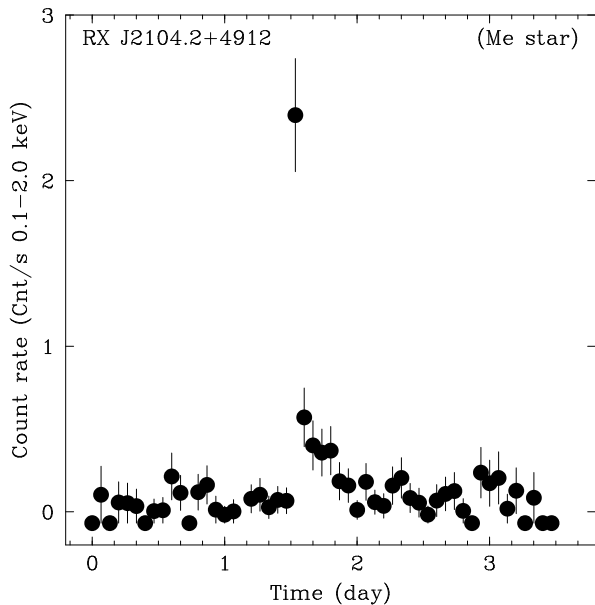


Fig. 13. X-ray flare from the Me star RX J2104.2+4912 (index 7). Few sources exhibit flaring-like activity and we conclude that there is probably no large bias favouring the preferential detection of particularly active stars

Table 6. Repartition in spectral types of all X-ray stars (giant and main sequence) with count rate ≥ 0.02 cts s^{-1} and located in the restricted 'inner' area

Spectral Type	Numbers	Percentages
A	6	14.3 ± 5.4
F	7	16.7 ± 5.7
G	11	26.2 ± 6.8
K	10	23.8 ± 6.5
M	8	19.0 ± 6.0
Total	42	100

10^9 yr) any coeval companion star will probably have a high X-ray activity as a result of its young age. However, ROSAT HRI observations seem to question this explanation and may point toward intrinsic X-ray emission in some late B stars (Berghöfer & Schmitt 1994). At the distance of the A stars the observed X-ray luminosities (see Fig. 14) are well in the range of those observed for classical active coronae. In two cases (RX J2056.7+4940, index 20 and RX J2117.8+5112, index 34) we obtained multicolour CCD images of the field but failed to identify a nearby likely alternative candidate. Assuming a limiting angular distance of $1''$ and a mean distance of 250 pc implies an upper limit of ≈ 250 AU on the projected separation of the two stars.

Only two giant stars HR 8252 (RX J2133.9+4535, index 2) and HR 8072 (RX J2103.4+5021, index 37) are present in our spectroscopically identified sample in agreement with the low spatial density and moderate X-ray luminosities of the evolved late type stars (Maggio et al. 1990).

The number of identified close systems is also small. We find evidences for a short period binary in two cases, RX J2107.3+5202 (index 26, V1061 Cyg; eclipsing F8+G1, $P = 2.3467$ d, Dworak 1976) and RX J2035.9+4900 (index 53, exhibiting a clear line doubling, Motch et al. 1996a). In a subsequent article we shall discuss in more detail the contribution of close binaries using as additional material red optical spectra covering the $\text{Li } \lambda 6707 \text{ \AA}$ line at a slightly higher resolution than that of the blue medium resolution spectra discussed here. In one additional case, RX J2120.9+4636 (index 9) we find conspicuous line doubling in the red medium resolution spectra indicating a close binary.

Our stellar X-ray population displays all the characteristics of an X-ray flux limited sample. We preferentially detect the high X-ray luminosity tail of the distribution function, several stars exhibiting X-ray luminosities in excess of $10^{30} \text{ erg s}^{-1}$ (see Fig. 14). X-ray luminosities were computed assuming negligible interstellar absorption and their estimated error is of the order of $\approx 40\%$ (Motch et al. 1996a). The mean X-ray luminosity clearly decreases with cooler photospheric effective temperature. This effect could be the result of a dependence of X-ray luminosity

with stellar radius (Fleming et al. 1989). We note that the only M star observed above 10^{30} erg s $^{-1}$ is the flaring source RX J2104.1+4912 (index 7, see Fig. 13) which would have been detected at about half of this luminosity in the absence of the flare. No particular spectral type dominates the stellar content of our survey area. Although the number density of dwarf G/K stars is only 10 to 16% that of dwarf M stars our distribution peaks at the G/K types. These number ratios indicate that the detection volume for G and K stars are about 14 and 8 times that of M stars and that accordingly, the mean X-ray luminosities of G and K stars are 5.7 and 4 times that of M stars. These figures are in general in good agreement with the mean Einstein X-ray luminosity ratios for disk stars (Micela et al. 1988, Barbera et al. 1993).

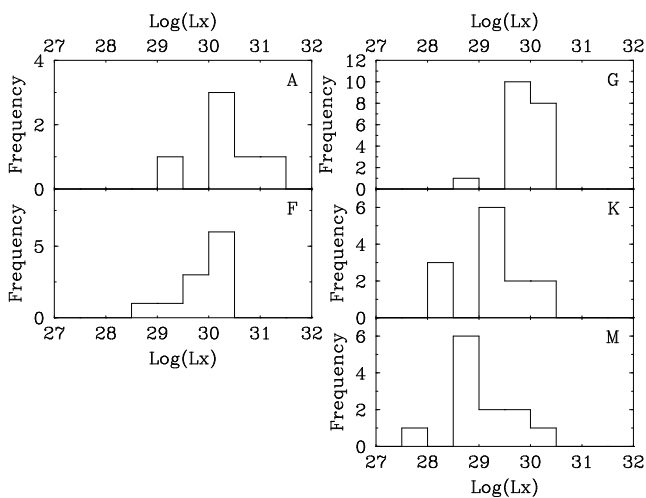


Fig. 14. Distribution in X-ray luminosities of all identified active coronae having spectral type information either from the literature or from our own optical observations. X-ray luminosities were computed assuming negligible interstellar absorption and a (0.1-2.4 keV) count to flux conversion factor of 1.0×10^{-11} erg cm 2 s $^{-1}$. As expected in an X-ray flux limited sample we preferentially sample the high luminosity tail of the X-ray luminosity function

Obviously, our survey maximum sampling distance also depends on the spectral type and we detect F stars up to 500 pc and M stars only up to ≈ 100 pc (see Fig. 15). Among the 24 open clusters recorded in SIMBAD in a $11^\circ \times 11^\circ$ region centered at $l = 90^\circ$, $b = 0^\circ$, only M39 at ($l = 92.5^\circ$, $b = -2.3^\circ$) is close enough ($d = 300 \pm 30$ pc; Mohan & Sagar 1985) to possibly introduce some inhomogeneity in our X-ray stellar sample. The relatively young age of the cluster (3 ± 1 10^8 yr, Mohan & Sagar 1985) indeed suggests that some active coronae could be detected. However, we do not observe any strong clustering of identified active coronae (see Fig. 16) nor unidentified sources

in that particular direction (see Fig. 22). Among the 4 X-ray stars detected within 1.5° from the center of the open cluster, only RX J2130.7+4919 (index 110) identified with Star 1930 in the Platais (1994) catalogue could be member of M39. Therefore, we believe that as far as active coronae are concerned our sample area is indeed representative of average mid galactic plane conditions.

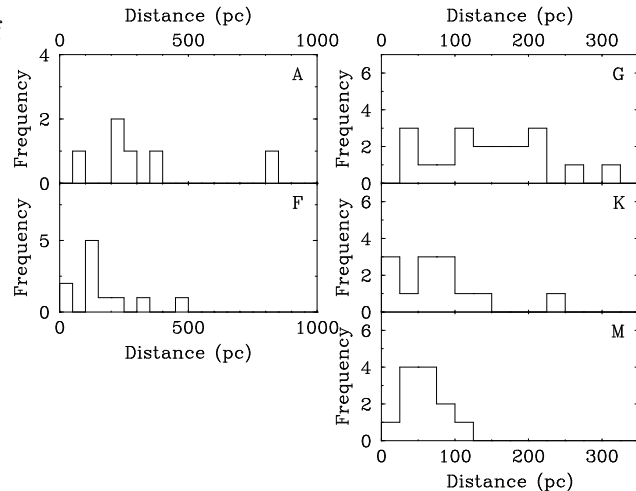


Fig. 15. Distribution in distance of all identified active coronae having spectral type information either from the literature or from our own optical observations

7. Accreting and related sources

Compared to other regions in the galactic plane this area in Cygnus is particularly void of accreting sources. The only catalogued X-ray binary is the low mass system 4U 2129+47 at $l = 91.58^\circ$ and $b = -3.04^\circ$ which is presently in an extended low state since the early 1980s (Pietsch et al. 1986). Our non detection is consistent with the faint ROSAT HRI source detected with a count rate of 0.004 cts s $^{-1}$ during a pointed observation which took place about one year after the survey observations (Garcia 1994). The only cataclysmic variable appearing in our source list is V1500 Cyg, also known as Nova Cyg 75, which is detected at the rather low maximum likelihood of 7.6.

We identify RX J2130.3+4709 (index 84) with a WD+Me star close binary. The blue optical spectrum (see Motch et al. 1996a) displays heavily broadened Balmer lines typical of a rather cool white dwarf with superimposed narrow Balmer and Ca II H&K emission lines. In the red, the spectrum is dominated by that of a late Me star with strong TiO molecular bands and H α emission. Radial velocities of Balmer absorption and emission lines vary in opposite directions with an orbital period of ≈ 12 hours. The white dwarf in RX J2130.3+4709 is too cool

Identified Active Coronae

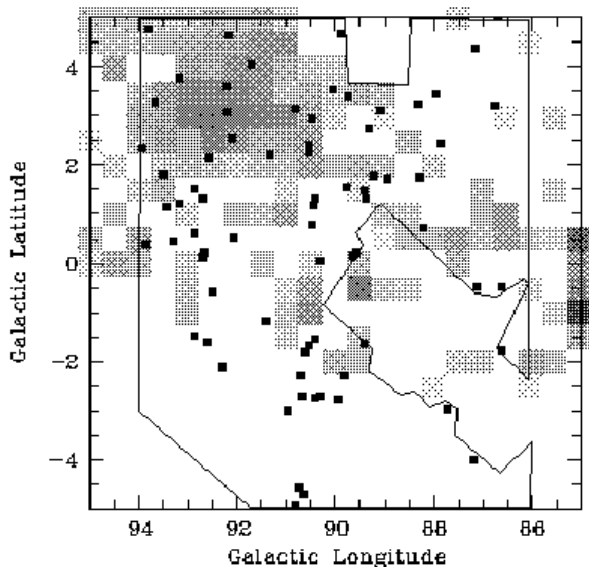


Fig. 16. Position of the identified active coronae (maximum likelihood ≥ 8) overlaid on the CO map from Dame et al. (1987) where we also show the area investigated in X-rays. Among the 24 open clusters present in a $11^\circ \times 11^\circ$ region centered at $l = 90^\circ$, $b = 0^\circ$, only M39 ($d \approx 300$ pc) at $l = 92.5^\circ$, $b = -2.3^\circ$ is close enough to be possibly detected at our sensitivity. The absence of concentration of sources at this position indicates that the presence of the cluster does not significantly bias the stellar statistics

to contribute to the X-ray emission and the flux detected by ROSAT ($1.6 \cdot 10^{-2}$ cts s^{-1}) probably arises from the Me star companion. In such a compact binary the late type star may be tidally locked to the white dwarf implying an enhanced rotational velocity and resulting coronal activity. RX J2130.3+4709 appears quite similar to RX J0458.9-6628 (Hutchings et al. 1995). We shall extensively discuss the properties of this system and its possible relation to cataclysmic variables in a forthcoming paper.

8. Extragalactic contamination

Although very low galactic fields such as the one investigated here are unlikely to contain a large fraction of extragalactic sources, our discovered AGN at $b = -3.4^\circ$ shows that this population is not completely screened out and may account for a significant fraction of the optically unidentified and relatively faint X-ray sources. In order to estimate this 'pollution' we assumed that the un-absorbed extragalactic $\log N(>S)$ - $\log S$ function was essentially that given in Hasinger et al. (1993). At our maximum possible flux sensitivity of $\approx 1\text{--}2 \cdot 10^{-13}$ erg cm^{-2} s^{-1} we are far

above the departure from the near Euclidean distribution and we may write the number of sources having X-ray flux within s and $s + ds$ as:

$$n(s) ds = N s^{-\beta} ds$$

However, our only measured quantity is the source count rate and for a given intrinsic spectrum the flux over count ratio may depend heavily on the intervening photoelectric absorption. In the Lockmann Hole (Hasinger et al. 1993) the soft X-ray flux is $s = k_0 \times c$ where c is the count rate measured from the source and the differential extragalactic count distribution is:

$$n(c) = N c^{-\beta} k_0^{1-\beta}$$

The observed count rate from sources dimmed by galactic absorption may be expressed as $c_a = K(\Omega) c$ where $K(\Omega)$ is the count absorption coefficient at position Ω . Averaging over the whole area and using the explicit form of the differential count distribution we may write:

$$n(c_a) = \frac{N c_a^{-\beta} k_0^{1-\beta}}{\Omega_0} \int_{\Omega_0} K(\Omega)^\beta d\Omega$$

Therefore, the absorbed extragalactic distribution has the same slope as the un-absorbed one but shifted to lower count rates.

We assumed a $\log N(>S)$ - $\log S$ (0.5-2 keV) relation with $N = 104$, $\beta = 2.44$ and an average spectrum of extragalactic sources in the form of a power law of energy index 0.96 (Hasinger et al. 1993, Gioia et al. 1990). We computed the count to flux ratios and count absorption coefficients for different values of the galactic absorption by folding the incident absorbed spectra with the detector response curve and by fitting a three degree polynomial to the $\log(K)/\log(N_H)$ relation. Because of the high photoelectric absorption we neglected the count rate resulting from the 0.1-0.5 keV low energy part of the spectrum. The galactic absorption was estimated from the HI maps of Strong et al. (1988) and Dame et al. (1987) interpolated on a 0.5° grid. The total N_H was taken as $N_{HI} + 2 \times 3.5 \cdot 10^{20} \times T_{CO}$ (e.g. Solomon & Rivolo 1987). Finally, the K coefficient was then integrated over the observed area.

Our simulation shows that on the average Cygnus field the count rate of extragalactic sources is only 15% of that detected at high galactic latitude and that at a given flux level we only detect 3.5% of the total extragalactic population. Table 7 lists the expected number of extragalactic sources as function of the absorbed count rates.

We have only one positive optical identification with a Seyfert 1 nucleus at a count rate of 0.1 cts s^{-1} (RX J2135.9+4728, index 12). Another source (RX J2133.3+4762, index 35) with a count rate of 0.035 cts s^{-1} is likely extragalactic. It has a very hard spectrum similar to that of the identified AGN and deep optical investigations fail to reveal the counterpart. We show in Fig.

Table 7. Absorbed extragalactic $\log N(>S)$ - $\log S$ function

count rate c_a 0.5-2 keV cnt s ⁻¹	$N (\geq c_a)$ 1 deg ²	$N (\geq c_a)$ 'full' area
0.01	$7.3 \cdot 10^{-2}$	4.7
0.02	$2.7 \cdot 10^{-2}$	1.7
0.03	$1.5 \cdot 10^{-2}$	1.0
0.05	$7.1 \cdot 10^{-3}$	0.45
0.10	$2.7 \cdot 10^{-3}$	0.17
0.50	$2.6 \cdot 10^{-4}$	0.02

17 the position of our two extragalactic candidates on a N_H map together with the investigated area. It is probably meaningful that our two non-galactic candidates fall into a region of very low absorption.

Considering the small number statistics, we believe that the number and count rates of our identified extragalactic candidates (2 sources with $c_a \geq 0.03$ cts s⁻¹) are in accord with our simulation. We conclude that the extragalactic population is likely to represent only a very small fraction ($\approx 3\%$) of the 68 sources detected in the 'full' area above our completeness level of 0.02 cts s⁻¹.

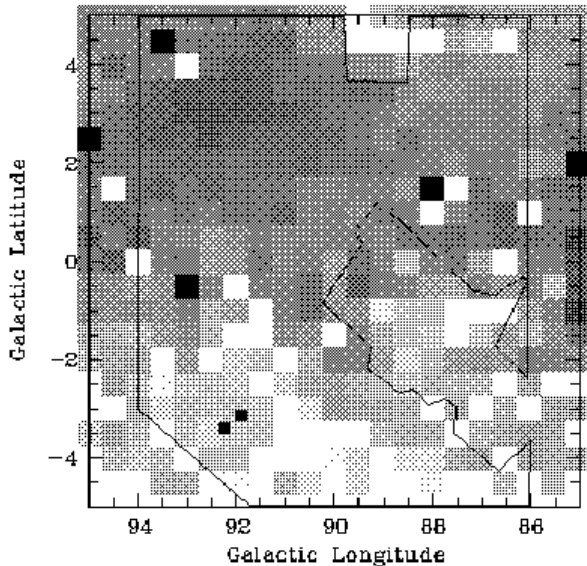


Fig. 17. A total N_H (HI + H₂) map (log grey scale) where we also show the region investigated in X-rays. N_H varies between $4.4 \cdot 10^{21}$ cm⁻² up to $4 \cdot 10^{22}$ cm⁻². Not surprisingly, our two extragalactic candidates (filled squares) fall in regions of low galactic absorption. We estimate that over the whole field shown here the extragalactic sources do not account for more than a few percent of the total population detected at a count rate above 0.02 cts s⁻¹.

9. Discussion

9.1. The $\log N(>S)$ - $\log S$ relation

We show in Fig. 18 the number count relation for all sources detected in the 'full' area above ML = 8 and ML = 10. From the bending of the $\log N(>S)$ - $\log S$ curve at low count rates we estimate that our total source sample is complete down to about 0.02 and 0.012 cts s⁻¹ for ML = 10 and 8 respectively. We note, however, that the enhanced number of spurious sources (see section 9.3) may complicate the definition of a completeness level at ML = 8. The corresponding source densities are 1.0 deg⁻² and 1.7 deg⁻² at 0.02 and 0.012 cts s⁻¹ respectively. In order to estimate the slope of the overall relation we used the maximum likelihood technique of Crawford et al. (1970) and Murdoch et al. (1973). For the 67 sources with ML ≥ 10 and count rate ≥ 0.02 cts s⁻¹, we find that:

$$N(\geq S) = 1.7 \times 10^{-2} S^{-1.05 \pm 0.13}$$

The slope and normalisation of the ROSAT survey relation is fully consistent with that reported by Hertz and Grindlay (1984) for the Einstein Galactic Plane Survey. Morley et al. (1996) also report compatible $\log N(>S)$ - $\log S$ relations from deep pointings in the galactic plane. As discussed in the previous section, the extragalactic contribution is probably negligible in our field. At high count rates the relative excess of sources is caused by few objects namely the three white dwarfs and our only identified AGN. In principle the slope of the white dwarf $\log N(>S)$ - $\log S$ function should be close to -1.5. In fact the lack of identified white dwarfs with count rates below 0.11 cts s⁻¹ could reflect the higher completeness flux level for this particular population resulting from the higher X-ray background at low energies. Alternatively we may see the large effects of tenuous interstellar absorption on such soft X-ray spectra.

Our high fraction of identified sources put us in a position to derive the $\log N(>S)$ - $\log S$ relation for stellar sources independently of the overall population. The inflexion of the $\log N(>S)$ - $\log S$ curve for the stellar X-ray sources also shown in Fig. 18 suggests that the identified stellar installment is roughly complete down to ≈ 0.03 cts s⁻¹ in the 'full' area, while the completeness level reaches 0.02 cts s⁻¹ in the 'inner' area (see sect. 6). Interestingly, we find that the $\log N(>S)$ - $\log S$ function of the optically identified active coronae is steeper than that of the total X-ray population. For the 41 sources with ML ≥ 10 and count rates above our estimated completeness level of identification (≈ 0.03 cts s⁻¹) we find a slope consistent with the Euclidean value.

$$N_{\text{stars}}(\geq S) = 3.6 \times 10^{-3} S^{-1.48 \pm 0.23}$$

This indicates that at the flux level of the ROSAT all-sky survey the distribution of the detected stellar population is not severely affected by interstellar absorption.

The Euclidean-like distribution is also consistent with the fact that in our low latitude test direction, the maximum distance above the plane (≈ 30 pc) of the most remote X-ray detections (≈ 300 pc) is much smaller than the scale height of any known group of late type stars.

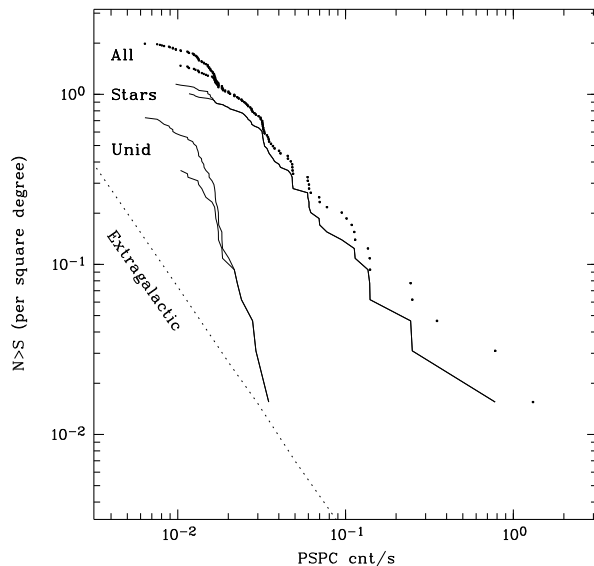


Fig. 18. The $\log N(>S)$ - $\log S$ function for sources with $ML \geq 10$ (lower curves) and $ML \geq 8$ (upper curves) in the 'full' area (64.5 square degrees). Above the completeness level of $\approx 0.02 \text{ cts s}^{-1}$ the slope of the distribution is close to -1. The identified stellar component has a slope of -1.48 ± 0.23 consistent with the Euclidean value for count rates above our identification completeness level of $\approx 0.03 \text{ cts s}^{-1}$. The dashed line represent the expected extragalactic contribution

9.2. X-ray counts modelling

Optical star count modelling is a very powerful mean to constrain several important parameters describing the various stellar populations of the Galaxy (e.g. Robin & Cr     1986). Because of the strong dependence of stellar X-ray emission with age, an X-ray view of the sky preferentially reveals the young stellar population. X-ray count modelling such as that developed by Favata et al. (1992) allows in particular the study of the local star forming rate during the last 10^9 yr, a field of investigation which is usually loosely constrained by optical star count analysis. Looking deep into the galactic plane has specific advantages since it allows to better constrain the youngest most luminous population which is concentrated in the low latitude regions of the galactic plane.

We first tried to compare our density of active coronae with the predictions of Favata et al. (1992). In their low

galactic latitude model ($b = 10^\circ$) the number of X-ray stellar source counts above $\log(F_X/\text{erg cm}^{-2} \text{ s}^{-1}) = -12.5$ corresponding to a PSPC count rate of $\approx 0.03 \text{ cts s}^{-1}$ is ~ 0.1 per square degree while our observed density is ≈ 0.6 . This rather large discrepancy could be related to the way the youngest stellar populations are treated.

In a second step we designed an age dependent numerical model by folding X-ray luminosity functions (XLFs) with the stellar population model of Robin & Cr     (1986). We used XLFs derived from ROSAT observations of the Pleiades and Hyades young galactic clusters and from Einstein observations of old disc population to handle the steeply varying stellar X-ray activity with age. Binaries are accounted for by using binary corrected luminosity functions. This X-ray model (fully described in Guillout et al. 1996a) allows to predict the distribution in age, spectral type, various colour indices, magnitudes and distance of the stellar content of X-ray flux limited or volume limited surveys. Detailed comparison of model predictions with observations in several low galactic latitude RASS areas will be discussed elsewhere and we only present here a preliminary analysis. Fig. 19 shows the computed $\log N(>S)$ - $\log S$ curves toward the direction of observation ($l = 90^\circ$, $b = 0^\circ$) for the standard model (stellar formation rate constant, slope of the initial mass function below $1 M_\odot = 0.7 \pm 0.2$) (Haywood 1995). The most interesting feature in Fig. 19 is the good agreement between observations and the predicted number counts curve. The departure at count rates below 0.02 cts s^{-1} is probably due to the incompleteness of our optical identifications. This suggests that in this sample region we clearly detect all the active stars expected on the basis of our current knowledge on stellar population and age dependent X-ray coronal activity.

Table 8 summarizes the model number of active coronae and the proportion of A, F, G, K, early and late M-type stars for various limiting PSPC count rate ($0.1 - 2.4 \text{ keV}$ band). For comparison, we list in Table 9 the distribution in spectral types of a completely identified stellar subsample made of the 40 main sequence stars located in the 'inner' area with $S \gtrsim 0.02 \text{ cts s}^{-1}$ together with the predicted distribution at the same flux limit. Considering the small number statistics, the observed distribution is in reasonable agreement with model predictions.

Another important feature shown in Fig. 19 is the outstanding importance of very young stars in the RGPS. For a limiting PSPC count rate $S = 0.03 \text{ cts s}^{-1}$ we expect that $\approx 65\%$ of the detected stellar X-ray sources are younger than 0.15 Gyr, this proportion increasing up to $\approx 85\%$ for stars younger than 1 Gyr (see Table 8). These first results indicate that stellar X-ray source counts may indeed be used to derive the basic properties of the young stellar populations and in particular put interesting constraints on the stellar formation rate (e.g. Micela et al. 1993, Guillout et al. 1996b).

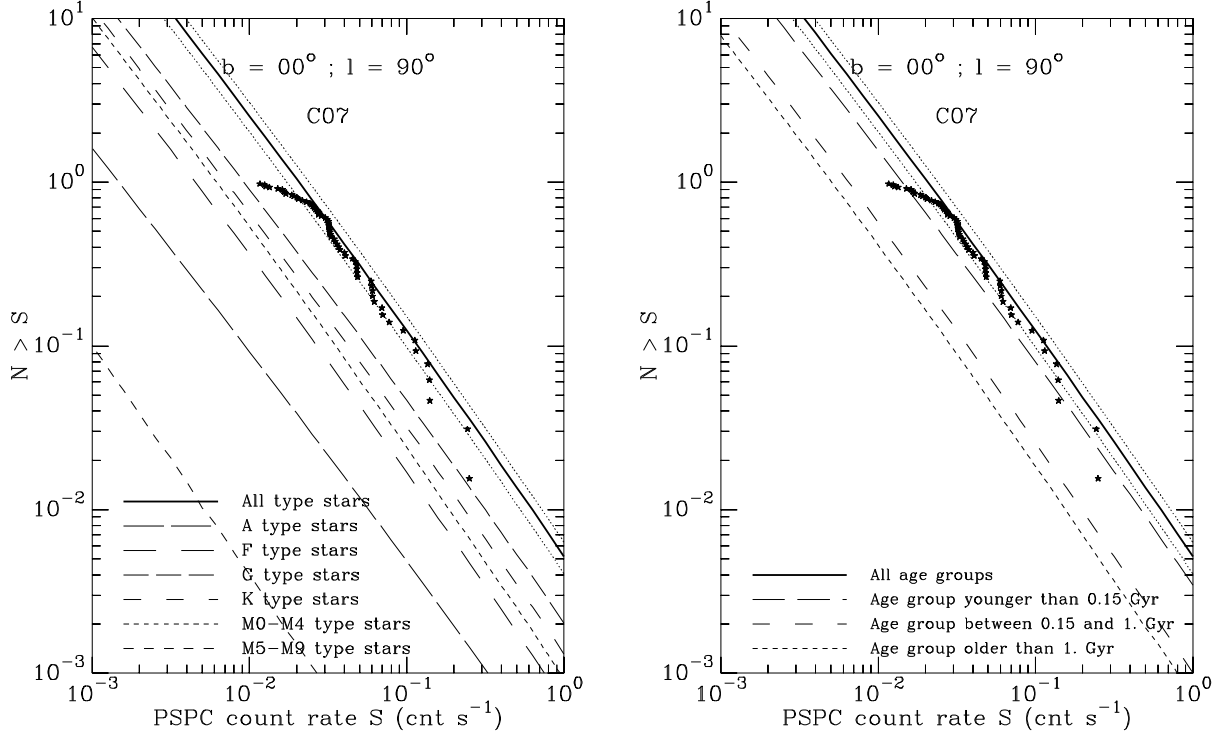


Fig. 19. Theoretical $\log N(>S)$ - $\log S$ curves for all stellar coronae (thick line), computed for the direction of the test area, assuming a constant stellar formation rate and a slope of the initial mass function below $1 M_{\odot}$ equal to 0.7 (C07). N is the number of stars per square degree in the direction l, b up to a given PSPC count rate S (0.1 - 2.4 keV band) as a function of the count rate. We also show the $\log N(>S)$ - $\log S$ curves computed separately for A, F, G, K and M type stars (a) - left panel) and various populations of disc stars (b) - right panel). The thin lines on both sides of the sum $\log N(>S)$ - $\log S$ curves represent the possible range resulting from the error due to the binning in age of the X-ray luminosity functions. The observed relation for all identified active coronae (giants excluded) with $ML \geq 10$ in the 'full' area is shown with asterisks

The X-ray count model used here ignores the contribution of giant stars which is expected to be small (Maggio et al. 1990). Another population not taken into account is that of close 'old' binaries. In these systems, the large rotation velocity maintained over the whole stellar life by tidal lock may sometimes yield large X-ray luminosity. However, the large uncertainties on the X-ray luminosity functions, spatial densities, mass ratio distributions of close binaries such as RS CVn systems (e.g. Ottmann & Schmitt 1992, Favata et al. 1995) do not allow to accurately estimate their specific contribution. Using the XLFs in Majer et al. (1986) and Favata et al. (1995), we estimate that more than 3% of the sources brighter than 0.02 cts s^{-1} could be active close binaries which is close to the observed fraction (4%) in our sample. However, as discussed in section 6, our follow-up observations are not very sensitive to binarity and the actual number of close systems may be somewhat larger.

9.3. Nature of the unidentified sources

Early simulations of survey data have shown that for a typical survey exposure the density of spurious sources was of the order of 0.0145 source per square degree above $ML = 10$ (Voges 1995). However, the precise number of false sources in a given survey field depends on background intensity and structure mainly determined by diffuse emission in our area. Consequently, the average figure mentioned above may be wrong by a factor of 2 or more in our case. The number of spurious sources per square degree detected above a given ML_0 may be estimated as:

$$N_{\text{spurious}}(ML \geq ML_0) = 1.45 \times 10^{-2} e^{10-ML_0}$$

This relation implies a formal density of spurious sources of 0.0145, 0.11 and 0.29 deg^{-2} for $ML_0 = 10, 8,$ and 7 respectively. Therefore, only 20% to 40% of the 0.53 unidentified sources per square degree with $ML \geq 8$ may be spurious. The expected extragalactic contribution com-

Table 8. Predicted number of stellar X-ray sources per square degree as a function of PSPC count rate (cts s⁻¹) in the direction of the Cygnus area. Also listed are the relative contributions in percents of various spectral types and age groups

Limiting PSPC count rate	3 10 ⁻²	1 10 ⁻²	1 10 ⁻³
Nbr of X-ray stars per deg ²	0.57	2.54	45.9
A	3.7	3.6	3.5
F	14.0	14.3	14.5
G	36.2	35.5	34.6
K	25.7	25.4	25.3
M0-M5	20.2	21.0	21.9
M6-M9	0.2	0.2	0.2
Age ≤ 0.15 Gyr	62.8	61.4	59.8
0.15 Gyr ≤ Age ≤ 1 Gyr	21.7	22.4	23.2
Age ≥ 1 Gyr	15.5	16.2	17.0

Table 9. Observed and predicted number of stellar X-ray sources per square degree and distribution in spectral types (percentages) for a limiting count rate of 0.02 cts s⁻¹.

	Observed	Model prediction
Nbr of X-ray stars per deg ²	1.05 ± 0.16	1.04
A	15.0 ± 5.6	3.7
F	17.5 ± 6.0	14.1
G	25.0 ± 6.8	36.0
K	22.5 ± 6.6	25.5
M0-M5	20.0 ± 6.3	20.5
M6-M9	–	0.2

Table 10. Density of unidentified sources

ML	Flux limit (cts s ⁻¹)	Total observed source density	Min-max model AC density	Identified non-AC	Unidentified	Possible range of unidentified non-AC non-extragalactic
10	0.020	1.02	0.84 – 1.41	0.10	0.10	0.0 – 0.09
8	0.012	1.74	1.32 – 2.66	0.10	0.53	0.0 – 0.29

puted in section 8 is also too weak to explain the remaining number of unidentified sources (see Fig. 18).

We list in Table 10 for two limiting count rates corresponding to the completeness levels for ML = 10 and ML = 8 several characteristic source densities (N(≥S) deg⁻²). Minimum and maximum model stellar densities were computed from the error due to binning in age of the XLFs and adding a ± 1σ source counting error in the 64.5 deg² area. In a similar manner we applied a - 1σ counting error to the estimated extragalactic contribution in the test region. The last column of Table 10 lists the maximum possible density range for the optically unidentified sources which are not associated with active coronae nor with extragalactic sources. These figures may be further lowered by the unknown fraction of spurious sources (up to 0.11 deg⁻² for ML=8). Using a density of active coronae extrapolated from the fitted logN(>S)-log S curve instead of the model prediction does not change the results. Considering the active coronae identified at the 95% confidence level on the basis of positional coincidence may allow to identify another 0.14 sources per square degree above 0.012 cts

s⁻¹. We conclude that there is no evidence for a large 'exotic' population in excess of 0.09 deg⁻² and 0.29 deg⁻² at 0.02 and 0.012 cts s⁻¹ respectively and that stars may well account for most if not all of the unidentified sources.

9.4. Constraints on X-ray emission from old neutron stars

As many as 10⁹ neutron stars could be born in the Galaxy during the last 10¹⁰ yr. After a relatively short lived radio emitting episode, these stellar remnants could reveal themselves in the EUV - soft X-ray energy bands if they accrete from the interstellar medium.

First proposed by Ostriker, Rees & Silk (1970) the possibility that such a population could appear in the current X-ray surveys has been recently studied by several authors. Treves & Colpi (1991) have discussed the case of magnetized neutron stars accreting from an homogeneous interstellar medium with particular emphasis put on the ROSAT PSPC instrument. Blaes & Madau (1993) have further studied the observability of old isolated neutron stars in a wide range of energies. They use a slightly different neutron star velocity distribution as Treves & Colpi

and consider several typical directions in the Galaxy representing the various distributions of hot tenuous and cool denser phases observed in the nearby interstellar medium. Colpi et al. (1993) have considered in more detail the case of the neutron stars accreting from dense molecular clouds.

Bondi accretion heavily depends on the relative velocity of the neutron star with respect to the interstellar medium and only the low velocity tail of the neutron star velocity distribution is expected to be detectable in X-rays. Another important parameter is the strength of the magnetic field which channels the accreted matter towards the poles and increases the effective temperature of the X-ray photons emerging from the polar cap.

The sensitivity of the ROSAT all-sky survey offers for the first time the possibility to sample this hypothetical population up to rather large distances over the whole sky. Treves & Colpi (1991) find that ~ 5000 old neutron stars spread almost isotropically over the sky should be present above a PSPC count rate of 0.015 cts s^{-1} which is the assumed sensitivity limit of the all-sky survey. Assuming a total number of $N_{\text{ns}} = 10^9$ neutron stars in the Galaxy, Blaes and Madau (1993) argue that at this level of X-ray flux, the number of detectable X-ray emitting members could be in the range from $\sim 2,000$ to $10,000$ depending on the accretion mode (polar or isotropic) with a marked concentration in the galactic plane.

We show in Fig. 20 and 21 the $\log N(>S)$ - $\log S$ function for our unidentified source fraction together with the various theoretical predictions.

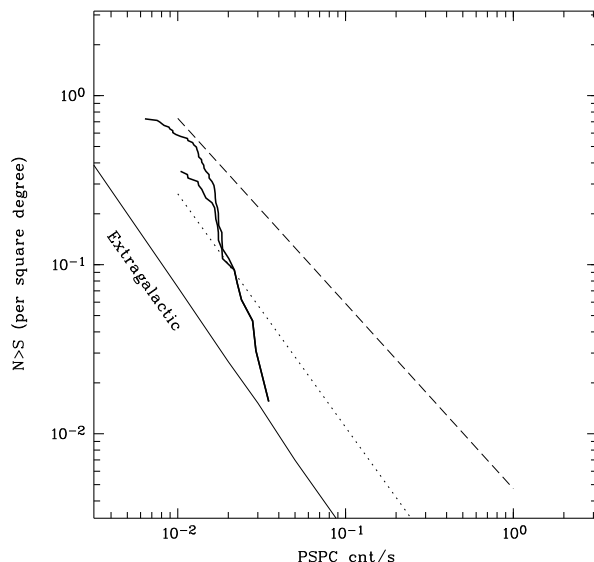


Fig. 20. The $\log N(>S)$ - $\log S$ relation for all unidentified sources with $ML \geq 8$ and $ML \geq 10$ (thick lines) in the 64.5 square degrees area. Over-plot are the predictions of Treves & Colpi (1991) for an interstellar density of $n = 0.07 \text{ cm}^{-3}$ (dotted line) and $n = 1 \text{ cm}^{-3}$ (dashed line)

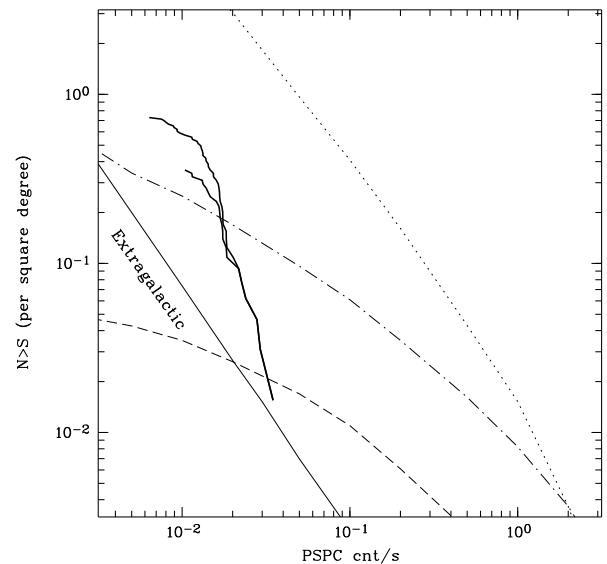


Fig. 21. The $\log N(>S)$ - $\log S$ relation for all unidentified sources with $ML \geq 8$ and $ML \geq 10$ (thick lines) in the 64.5 square degrees area. Over-plot are the predictions of Blaes & Madau (1993); Case 1 polar (dotted line), Case 1 isotropic (dotted dashed line) and Case 4 polar (dashed line)

Our observed $\log N(>S)$ - $\log S$ relation for unidentified sources and the upper limits listed in Table 10 clearly rule out the $n = 1 \text{ cm}^{-3}$ density case of Treves & Colpi and are marginally compatible with the $n = 0.07 \text{ cm}^{-3}$ density case. More stringent constraints may be put on the model of Blaes & Madau (1993) ($N_{\text{ns}} = 10^9$) since we can exclude their case 1 thought to be representative of the galactic plane whatever is the accretion mode polar or isotropic.

The enhanced density of the interstellar medium in molecular clouds favours the detection of accreting neutron stars in their direction. Colpi, Campana & Treves (1993) estimated that the CYG OB7 cloud which is the dominant CO feature in our area could harbour as many as 1000 lonely accreting neutron stars. Fig. 4 shows that we cover a very large fraction of this molecular cloud, especially the densest parts. These authors estimate that ≈ 70 neutron stars with accretion luminosity of the order of $10^{32} \text{ erg s}^{-1}$ could be detected above 0.02 cts s^{-1} . Our detection at similar count rates of X-ray emission from two bright OB stars probable members of CYG OB7 shows that we are indeed sensitive to accreting neutron stars located in this molecular cloud. Our observations seem to be at variance with predictions since at the level of 0.02 cts s^{-1} , we only have 8 unidentified sources over the whole field (see Table 3) instead of the expected 72 for the entire cloud or 36 for a half cloud. We show in Fig. 22 the position of the unidentified sources overlayed on the CO map (Dame et al. 1987). The absence of correlation between the location of unidentified sources and CO intensity seems indeed incompatible with the idea that the

majority of these sources are old neutron stars accreting from the dense interstellar medium. However, we cannot completely rule out a conspiracy resulting from the correlation between high X-ray luminosities and photoelectric absorption. In a recent paper, Zane et al. (1995) perform a more accurate analysis of the distribution of old neutron star. Assuming the most favourable cases of polar cap accretion, they predict that ≈ 9 to 17 such sources may be detected in the entire CYG OB7 above 0.02 cts s^{-1} . This reduced number is now compatible with our observations.

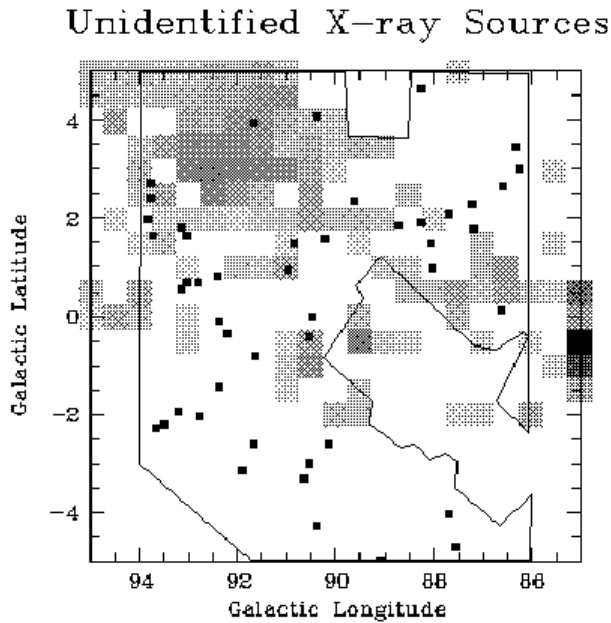


Fig. 22. Position of the unidentified X-ray sources (maximum likelihood ≥ 8 , all count rates) overlayed on the CO map from Dame et al. (1987) where we also sketch the area investigated in X-rays. The absence of a correlation between the distribution of the unidentified population and the CO structures seems to rule out the possibility that these sources consist of a majority of extragalactic sources or of lonely neutron stars accreting from the dense interstellar medium. The $\log N(>S)$ - $\log S$ function and the spatial repartition rather suggest that most unidentified sources are active coronae

Considering the various ingredients entering these models the lack of a large population of unidentified, old neutron star candidate X-ray sources may have one or several different interpretations.

The first important parameter is the density of the interstellar medium in the direction surveyed here. Because of the very low density of the local cavity ($n_H \leq 0.015 \text{ cm}^{-3}$) in which the Sun seems presently embedded and which extends at least up to 50 pc in most directions (Paresce 1984, Welsh et al. 1994), we do not expect the

presence of nearby X-ray luminous lonely neutron stars (Blaes & Madau 1993). At larger distances from the Sun, the mean density of the interstellar medium reaches more typical values for the Galaxy ($n_H \approx 1.0 \text{ cm}^{-3}$, Blaes & Madau 1993). Although there exists some general agreement on the main structure of the local bubble, namely a large extent toward galactic longitudes $l = 200$ - 270° , the details of the boundary are poorly known. However, Welsh et al. (1994) claim that the bubble radius could be as narrow as 25 pc toward $l = 90^\circ$ and Paresce (1984) find consistent results although with a lower spatial resolution (see also Zane et al. (1996) for a recent discussion of the local interstellar medium). The maps of interstellar extinction from Neckel & Klare (1980) show that in most directions concerned here A_V smoothly increases to ≈ 1 at 1 kpc and that in the innermost regions of the plane the interstellar absorption already reaches $A_V \approx 2.5$ at 500 pc. This indicates a mean hydrogen density in the range of 0.6 - 3.0 cm^{-3} up to a few hundreds of parsecs. We conclude that in the direction surveyed here in X-rays the interstellar medium has a density and a radial distribution typical of the mid-plane conditions as defined by Blaes & Madau (1993) and that the correct models to compare with are those of case 1 (see Fig. 21).

Following Madau & Blaes (1994) we argue that the second crucial parameter is the velocity distribution of the old neutron stars since the most powerful X-ray sources will be those few with very low velocities relative to the interstellar medium. If the mechanism increasing the velocity dispersion of old stars (Wielen 1977) is also at work for old neutron stars, the number of low velocity neutron stars may be severely overestimated. Finally, the overall number of neutron stars assumed to be born in the Galaxy may also be overestimated.

Madau & Blaes (1994) demonstrated that a model taking into account the dynamical heating of the old neutron star population would indeed drastically decrease the detectability of these objects in the RASS. Following their computations, our limit on the density of non-coronal non-extragalactic sources could imply an overall number of old neutron stars of only ($N_{ns} \approx 10^8$) if accretion always occurs on polar caps. Alternatively, a large number of fossil neutron stars ($N_{ns} = 10^9$) would only be acceptable if accretion occurs isotropically and if the dynamical heating mechanism is at work. Based on results from the EUVE and WFC all-sky surveys and using an early report on a parallel optical identification program of RASS sources carried out by our group in the Taurus constellation (Guillout et al. 1996b), Madau & Blaes (1994) concluded that the presently available observations may already hint at a much less numerous old neutron star population than previously thought. The present constraints, however, do not preclude the discovery of few relatively close (≈ 100 pc) isolated neutron stars (e.g. Walter et al. 1996).

10. Conclusions

We present the first results of a systematic identification programme of ROSAT all-sky survey sources in the galactic plane. The test region analyzed in this paper was chosen to be typical of deep plane conditions. Centered at $l = 90^\circ$ $b = 0^\circ$ it contains 128 sources above a maximum likelihood of 8 in a 64.5 deg^2 area. The overall $\log N(>S)$ - $\log S$ function is fully consistent with that derived from the Einstein galactic plane surveys having similar X-ray sensitivity (Hertz & Grindlay 1984) and with the results of deep ROSAT pointings (Morley et al. 1996). Thanks to a high completeness of optical identifications we are in a position to discuss the relative contributions of various kinds of X-ray sources. An overwhelming fraction of X-ray sources are identified with late type active coronae. Our identified sample exhibits the X-ray luminosity distribution expected in a flux limited survey and we detect F-G stars up to $\approx 300 \text{ pc}$ while M stars are not found beyond $\approx 100 \text{ pc}$. X-ray count models account satisfactorily both for the observed $\log N(>S)$ - $\log S$ relation and for the distribution in spectral types and suggest that most of the stars detected by ROSAT in this low latitude region are probably younger than 1 Gyr. We also put strong constraints on the possible contributions of old neutron stars accreting from the interstellar medium and discuss the possible implications of our results.

Acknowledgements. We thank A. Strong for kindly providing the CO and HI maps in electronic form. We thank the night assistants at Observatoire de Haute-Provence for carrying out some of the observations at the 1.2m telescope. The ROSAT project is supported by the Bundesministerium für Bildung, Wissenschaft, Forschung und Technologie (BMBF/DARA) and the Max-Planck-Gesellschaft. C.M. acknowledges support from a CNRS-MPG cooperation contract and thanks Prof. J. Trümper and the ROSAT group for their hospitality and fruitful discussions. This research has made use of the SIMBAD database operated at CDS, Strasbourg, France.

References

- Barbera, M., Micela, G., Sciortino, S., Harnden, F.R., Rosner, R., 1993, *ApJ* 414, 846
- Berghöfer, T.W., Schmitt, J.H.M.M., 1994, *A&A* 292, L5
- Blaes, O., Madau, P., 1993, *ApJ* 403, 690
- Cash, W., Charles, P., Bowyer, S., Walter, F., Garmire, G., Riegler, G., 1980, *ApJ* 238, L71
- Colpi, M., Campana, S., Treves, A., 1993, *A&A* 278, 161
- Crawford, D.F., Jauncey, D.L., Murdoch, H.S., 1970, *ApJ* 162, 405
- Dame, T.M., Thaddeus, P., 1985, *ApJ* 297, 751
- Dame, T.M., Ungerechts, H., Cohen, R.S., De Geus, E.J., Grenier, I.A., May, J., Murphy, D.C., Nyman, L.Å., Thaddeus, P., 1987, *ApJ* 322, 706
- Dworak, T.Z., 1976, *IAU Inform. Bull. Var. Stars*, 1136, 1
- Favata, F., Micela, G., Sciortino, S., Vaiana, G.S., 1992, *A&A* 256, 86
- Favata, F., Micela, G., Sciortino, S., 1995, *A&A* 298, 488
- Feitzinger, J.V., Stüwe, J.A., 1986, *Vistas in Astronomy*, Vol. 29, p291.
- Fleming, T.A., Liebert, J., Gioia, I.M., Maccacaro, T., 1988, *ApJ* 331, 958
- Fleming, T.A., Gioia, I., Maccacaro, T., 1989, *ApJ* 340, 1011
- Garcia, M.R., 1994, *ApJ* 435, 407
- Georgelin, Y.M., Georgelin, Y.P., 1976, *A&A* 49, 57
- Gioia, I.M., Maccacaro, T., Schild, R.E., Stocke, J., Liebert, K., Danziger, I., Kunth, D., Lub, J., 1984, *ApJ* 283, 495
- Gioia, I.M., Maccacaro, T., Schild, R.E., Wolter, A., Stocke, J.T., Morris, S.L., Henry, J.P., 1990, *ApJS* 72, 567
- Guillout, P., 1996, Ph.D. Thesis, Strasbourg, Université Louis Pasteur
- Guillout, P., Haywood, M., Motch, C., Robin, A.R., 1996a, *A&A* in press
- Guillout, P., Haywood, M., Motch, C., Robin, A.R., 1996b, in proceedings of the conference "Röntgenstrahlung from the Universe", Würzburg, Germany, September 25-29 1995
- Haberl, F., Thorstensen, J.R., Motch, C., Schwarzenberg-Czerny, A., Pakull, M., Shambrook, A., Pietsch, W., 1994, *A&A* 291, 171
- Haberl, F., Motch, C., 1995, *A&A* 297, L37
- Hasinger, G., Burg, R., Giacconi, R., Hartner, G., Schmidt, M., Trümper, J., Zamorani, G., 1993, *A&A* 275, 1
- Haywood, M., 1995, Ph. D. Thesis, Paris, Université Paris-VI
- Hertz, P., Grindlay, J., 1984, *ApJ* 278, 137
- Hertz, P., Grindlay, J., 1988, *AJ* 96, 233
- Hutchings, J.B., Crampton, D., Cowley, A.P., Schmidtke, P.C., McGrath, T.K., Chu, Y.-H., 1995, *PASP* 107, 931
- Kulkarni, S.R., Blitz, L., Heiles, C., 1982, *ApJ* 259, L63
- Lanning, H.H., Meakes, M., 1994, *PASP* 106, 38
- Lasker, B.M., Sturch, C.R., McLean, B.J., Russel, J.L., Jenkner, H., Shara, M.M., 1990, *AJ* 99, 2019
- Madau, P., Blaes, O., 1994, *ApJ* 423, 748
- Maggio, A., Sciortino, S., Vaiana, G.S., Majer, P., Bookbinder, J., Golub, L., Harnden, F.R., Rosner, R., 1987, *ApJ* 315, 687
- Maggio, A., Vaiana, G.S., Haisch, B.M., Stern, R.A., Bookbinder, J., Harnden, Jr., F.R., Rosner, R., 1990, *ApJ* 348, 253
- Majer, P., Schmitt, J.H.M.M., Golub, L., Harnden, F.R., Rosner, R., 1986, *ApJ* 300, 360
- Micela, G., Sciortino, S., Vaiana, G.S., Harnden, F.R., Rosner, R., Schmitt, J.H.M.M., 1988, *ApJ* 348, 557
- Micela, G., Sciortino, S., Favata, F., 1993, *ApJ* 412, 618
- Mohan, V., Sagar, R., 1985, *MNRAS* 213, 337
- Morley, J.E., Pye, J.P., Warwick, R.S., Pilkington, J., 1996, in proceedings of the conference "Röntgenstrahlung from the Universe", Würzburg, Germany, September 25-29 1995
- Motch, C., Belloni, T., Buckley, D., Gottwald, M., Hasinger, G., Pakull, M.W., Pietsch, W., Reinsch, K., Remillard, R.A., Schmitt, J.H.M.M., Trümper, J., Zimmermann, H.-U., 1991, *A&A* 246, L24
- Motch, C., 1992, MPE report MB-ROS-ME-MA00/185,14
- Motch, C., Hasinger, G., Pietsch, W., 1994, *A&A* 284, 827
- Motch, C., Guillout, P., Haberl, F., Pakull, M., Pietsch, W., Reinsch, K. 1996a, *A&A* in press
- Motch, C., Haberl, F., Dennerl, K., Pakull, M., E. Janot-Pacheco, 1996b, preprint
- Murdoch, H.S., Crawford, D.F., Jauncey, D.L., 1973, *ApJ* 183, 1

- Neckel, Th., Klare, G., 1980, A&AS 42, 251
- Nugent, J.J., Jensen, K.A., Nousek, J.A., Garmire, G.P., Mason, K.O., Walter, F.M., Bowyer, C.S., Stern, R.A., Riegler, G.R., 1983, ApJS 51, 1
- Ostricker, J., Rees, M.J., Silk, J., 1970, Astrophys. Lett., 6, 179
- Ottmann, R., Schmitt, J.H.M.M., 1992, A&A 256, 421
- Pallavicini, R., P., Golub, L. Rosner, R., Vaiana, G.S. Ayres, T., Linsky, J.L., 1981, ApJ 248, 279
- Paresce, F., 1984, AJ 89, 1022
- Pfeffermann, E., Briel, U.G., Hippmann, H., Kettenring, G., Metzner, G., Predehl, P., Reger, G. Stephan, K.H., Zombeck, M.V., Chappell, J., Murray, S.S., 1986, SPIE, 733, 519
- Pietsch, W., Steinle, H., Gottwald, M., Graser, U., 1986, A&A 157, 23
- Pirenne, B., Albrecht, M., Durand, D., Gaudet, S., 1993, in *Astronomical Data Analysis Software and Systems II*, Eds Hanish R. J., Brissenden R. J. V., Barnes J., Proceedings, Astronomical Society of the Pacific, 95, 99
- Platais, 1994, Bull. Inf. Centre de Données Stellaires, 44, 9
- Preite-Martinez, A., Ochsenbein, F., 1993, in Proceedings of the ESO/OAT Workshop on Handling and Archiving Data from Ground-based Telescopes, Eds F. Pasian & M. Albrecht
- Reimers, D., 1989, p53, in "GFK stars and TTauri stars", NASA SP-502, Eds Cram, L.E., Kuhi, L.
- Robin, A., Cr    , M., 1986, A&A 157, 71
- Rosner, R., Golub, L., Vaiana, G.S., 1985, ARAA, 23, 413
- Rutten, R.G.M., Schrijver, C.J., Zwaan, C., Duncan, D.K., Mewe, R., 1989, A&A 219, 239
- Schmitt, J.H.M.M., Collura, A., Sciortino, S., Vaiana, G.S., Harnden, F.R., Rosner, R., 1990, ApJ 365, 704
- Schrijver, C. J., 1983, A&A 127, 289
- Skumanich, A., Young, A., Stauffer, J., Bopp, B.W., 1984, BAAS, 16, 940
- Snowden S.L., Freyberg M.J., Plucinsky P.P., Schmitt, J.H.M.M., Tr    per, J., Voges, W., Edgar, R.J., McCammon, D., Sanders, W., 1995, ApJ 454, 643
- Solomon, P.M., Rivolo, A.R., 1987, in *The Galaxy*, Eds G.Gilmore and B. Carswell, p105
- Stoeke, J.T., Morris, S.L., Gioia, I.M., Maccacaro, T., Schild, R., Wolter, A., Fleming, T., Henry, J.P., 1991, ApJS 76, 813
- Strong, A.,W. Bloemen, J.B.G.M., Dame, T.M., Grenier, I.A., Hermesen, W., Lebrun, F.,Nyman, L.-A., Pollock, A.M.T., Thaddeus, P., 1988, A&A 207, 1
- Treves, A., Colpi, M., 1991, A&A 241, 107
- Tr    per, J., 1983, Adv. Space. Res., 2, 241
- Vaiana, G.S., Cassinelli, J.P., Fabbiano, G., Giacconi, R., Golub, L., Gorenstein, P., Haisch, B.M., Harnden, F.R., Johnson, H.M., Linsky, J.L., Maxson, C.W., Mewe, R., Rosner, R., Seward, F., Topka, K., Zwaan, C., 1981, ApJ 245, 163
- Voges, W., 1992, in Proceedings of Satellite Symposium 3, 'International Space Year Conference', ESA ISY-3, p. 9
- Voges, W., Gruber, R., Paul, J., Bickert, K., Bohnet, A., Bur-sik, J., Dennerl, K., Englhauser, J., Hartner, G., Jennert, W., K    ler, H., Rosso, C., 1992, in Proceedings of Satellite Symposium 3, 'International Space Year Conference', ESA ISY-3, p. 1
- Voges, W., 1995, private communication
- Vogt, N., Moffat, A.F.J., 1975, A&A 39, 477
- Walter, F.M., Wolk, S.J., Neuh    ser, R., 1996, Nat 379, 233
- Warwick, R.S., Turner, M.J.L., Watson, M.G., and Willingale, R., 1985, Nat 317, 218
- Wielen, R., 1977, A&A 60, 263
- Welsh, B.Y., Craig, N., Vedder, P.W., Vallerger, J.V., 1994, ApJ 43, 638
- Wesemael, F., Greenstein, J.L., Liebert, J., Lamontagne, R., Fontaine, G., Bergeron, P., Glapsey, J.W., 1993, PASP 105, 761
- Wilson, O.C., 1963, ApJ 138, 832
- Wilson, O.C., 1966, ApJ 144, 695
- Wood K.S., Meekins J.F., Yentis D.J., Smathers H.W., Mcnutt D.P., Bleach R.D., Byram E.T., Chubb T.A., Friedmann H. and Meidav M., 1984, ApJS 56,507,
- Zane, S., Turolla, R., Zampieri, L., Colpi, M., Treves, A., 1995, ApJ 451, 739
- Zane S., Zampieri L., Turolla R., Treves A., 1996, A&A 309, 469
- Zickgraf, F.-J., Thiering, I., Krautter, J., Appenzeller, I., Kneer, R., Voges, W., Serrano, A., Mujica, R., 1996, in proceedings of the conference "R    ngenstrahlung from the Universe", W    zburg, Germany, September 25-29 1995
- Zickgraf, F.-J., 1996, private communication
- Zimmermann, H.U., Belloni, T., Izzo, C. Kahabka, P., Schwen-tker, O., 1992, MPE Report 48.

Note added in proof: After the paper was accepted for publication, a new search in SIMBAD revealed that RX J2134.2+4911 (index 97) is most probably identified with the dwarf nova V1081 Cyg.

Table 11. Optical identifications for sources with $ML \geq 8$. Entries are sorted by decreasing count rates. For the sake of completeness, we also list the proposed counterparts having a probability of identification in the range 95% - 98%. These more uncertain cases are marked by a '?' as first letter of the identification name and the class acronym is followed by a '?'

1	RX J2112.7+5006	WD	DAw	GD 394	1.310	0.041	3643.6	1.00	–
2	RX J2133.9+4535	AC	G8III	HR 8252	0.779	0.035	1297.3	1.00	–
3	RX J2052.7+4639	WD	DO	C	0.351	0.021	863.4	1.00	–
4	RX J2125.2+4942	AC	K4V	A =GSC-0359801594	0.250	0.019	422.2	1.00	0.30
5	RX J2100.8+4530	AC	G3V	SAO 50350	0.244	0.017	425.1	1.00	0.70
6	RX J2106.0+5421	AC	F8V	HD 235440	0.140	0.017	106.2	1.00	< 0.04
7	RX J2104.1+4912	AC	M4e	B	0.139	0.014	267.3	1.00	–
8	RX J2130.8+4827	AC	G3V	SAO 50961	0.136	0.015	168.7	1.00	< 0.18
9	RX J2120.9+4636	AC	F9V	A =GSC-0358903858	0.114	0.013	150.5	1.00	0.64
10	RX J2124.7+4639	AC	K3+K7V	A+B	0.113	0.013	159.4	1.00	0.59
11	RX J2117.3+5044	WD	DA	B =LAN 121	0.109	0.013	105.3	1.00	–
12	RX J2135.9+4728	AGN	Seyf 1	B	0.101	0.012	160.4	1.00	–
13	RX J2102.6+4552	AC	K3V	HD 200560	0.095	0.011	168.8	1.00	–
14	RX J2123.1+4831	AC	F0V	HD 203839	0.077	0.011	81.2	1.00	< 0.92
15	RX J2055.3+5025	AC	G0V	A =GSC-0358301038	0.070	0.012	58.8	1.00	< 0.01
16	RX J2109.2+4810	AC	K7V	A =GSC-0359205781	0.070	0.011	68.3	0.98	0.85
17	RX J2100.9+5103	AC	M2Ve	A =G 231 -24	0.062	0.011	51.8	1.00	–
18	RX J2049.6+5119	AC	F2V	HD 198638	0.061	0.011	46.4	1.00	–
19	RX J2059.3+5303	AC	M3.5Ve	A =GSC-0395201062	0.061	0.012	38.8	1.00	–
20	RX J2056.7+4940	AC	A7V	SAO 50269	0.060	0.010	61.7	1.00	–
21	RX J2123.1+5021	AC	G0V	A =BD+49 3512	0.059	0.010	52.2	1.00	0.19
22	RX J2107.8+4932	AC	G8V	A =GSC-0359600261	0.049	0.009	44.6	1.00	0.77
23	RX J2100.1+4841	AC	G9V	BD+48 3260 E	0.048	0.009	37.4	0.99	0.44
24	RX J2104.7+5223	AC	G2V	A =GSC-0360000513	0.048	0.011	33.0	0.99	0.04
25	RX J2044.6+4758	AC		A =GSC-0357800872	0.048	0.009	49.6	0.99	–
26	RX J2107.3+5202	AC	F8V	V1061 Cyg =HD 235444	0.047	0.010	40.1	1.00	–
27	RX J2052.3+4820	AC	G9V	A =GSC-0357901469	0.045	0.009	43.8	0.99	0.64
28	RX J2118.4+4356	OB	O8Ve	HR 8154	0.045	0.009	48.6	1.00	–
29	RX J2109.3+5138	AC	G3V	A =GSC-0360000175	0.041	0.009	29.7	1.00	0.53
30	RX J2120.4+4733	AC	K4V	HD 203418	0.040	0.008	34.9	1.00	0.91
31	RX J2104.2+5015	AC	K7e	A	0.038	0.008	16.0	1.00	–
32	RX J2057.3+4813	AC	A2m	A =GSC-0357900338	0.037	0.008	33.6	0.99	< 0.11
33	RX J2119.0+5207	AC	G1V	A =GSC-0360101235	0.036	0.009	32.3	0.99	0.20
34	RX J2117.8+5112	AC	A2V	HD 203028	0.035	0.008	20.7	1.00	–
35	RX J2133.3+4726	??			0.035	0.008	41.8	0.00	–
36	RX J2134.0+4525	AC	G3V	A =GSC-0359101945	0.034	0.010	16.0	0.99	0.60
37	RX J2103.4+5021	AC	K0III	HR 8072	0.034	0.008	35.0	1.00	0.96
38	RX J2040.6+4859	AC	F9V	SAO 49928	0.033	0.008	38.4	1.00	< 0.17
39	RX J2102.9+4854	AC	G3V	A =GSC-0359600374	0.033	0.008	24.1	0.99	0.49
40	RX J2113.3+5140	AC	M4Ve	A	0.032	0.008	42.9	1.00	–
41	RX J2123.5+4621	AC	K4V	A =GSC-0359002325	0.032	0.008	28.1	0.98	0.63
42	RX J2100.9+4857	AC	K2V	A =GSC-0359601318	0.032	0.008	23.5	0.00	0.08
43	RX J2130.1+4901	AC	M5Ve	B	0.032	0.008	26.6	1.00	0.03
44	RX J2054.1+4942	AC	F8V	A =GSC-0358300309	0.032	0.009	14.8	0.99	< 0.01
45	RX J2116.6+4645	AC	M5Ve	A	0.032	0.008	29.7	1.00	0.28
46	RX J2110.2+5333	OB	Ap	HR 8106	0.031	0.010	18.4	1.00	–
47	RX J2125.3+4642	AC	F0V	HR 8208	0.031	0.008	26.0	1.00	–
48	RX J2118.5+5247	AC		A =GSC-0395301190	0.030	0.008	23.0	0.99	–
49	RX J2128.7+4409	??			0.029	0.009	10.4	0.00	–
50	RX J2121.7+5049	AC	A0V	HD 235498	0.029	0.008	28.0	1.00	< 0.95
51	RX J2132.5+4849	??			0.028	0.008	19.7	0.94	< 0.02
52	RX J2122.4+5023	AC	G9V	A =GSC-0359700228	0.028	0.008	22.2	0.97	0.46
53	RX J2035.9+4900	AC	G5-8V	A =GSC-0358101856	0.027	0.007	22.5	0.99	0.75
54	RX J2108.2+5313	AC	A0V	HD 201543	0.027	0.009	15.2	1.00	–
55	RX J2128.6+4653	AC	K5V	A =GSC-0359400075	0.026	0.007	21.7	0.93	0.59
56	RX J2048.0+4903	AC		A =GSC-0358200586	0.026	0.007	27.5	0.99	–
57	RX J2115.4+4437	AC	K0V	A =GSC-0318101403	0.025	0.007	20.7	0.98	0.98
58	RX J2109.9+4809	AC	A5V	SAO 50523	0.025	0.007	16.1	1.00	–
59	RX J2108.6+4927	AC	M2Ve	A	0.024	0.007	22.9	1.00	0.17
60	RX J2050.8+4743	??			0.024	0.007	21.0	0.84	–
61	RX J2135.6+4523	AC	F9V	A =GSC-0359102803	0.023	0.008	10.6	0.00	0.06
62	RX J2119.9+5227	AC?		? A =GSC-0360101367	0.023	0.007	23.4	0.98	–
63	RX J2100.3+5219	AC	M1Ve	A =GSC-0360000514	0.022	0.008	19.0	1.00	–
64	RX J2056.3+4817	??			0.022	0.007	13.5	0.00	–
65	RX J2127.3+5121	AC		A+B	0.020	0.007	21.1	0.99	–
66	RX J2041.9+4746	??			0.020	0.007	8.4	0.00	–
67	RX J2126.3+4654	AC		A =GSC-0359401755	0.020	0.007	10.2	0.98	–
68	RX J2055.8+5044	AC	G8V	A =GSC-0358700365	0.019	0.007	15.1	0.97	0.23
69	RX J2117.5+5127	AC	M0Ve	A =GSC-0360100450	0.019	0.007	12.8	1.00	–
70	RX J2057.7+4752	??			0.018	0.006	11.3	0.00	–
71	RX J2131.2+4533	??			0.018	0.007	9.3	0.00	–
72	RX J2054.6+5120	??			0.018	0.006	12.0	0.93	< 0.01
73	RX J2121.5+4317	??			0.018	0.006	8.2	0.00	–
74	RX J2128.4+4900	??			0.017	0.006	10.5	0.00	–
75	RX J2058.5+4836	??			0.017	0.006	10.7	0.92	–
76	RX J2130.0+4740	AC?	K4V	? A =Plat 2137	0.017	0.006	12.6	0.97	–
77	RX J2106.2+4437	AC	M5Ve	A	0.017	0.006	16.7	1.00	0.33
78	RX J2128.5+4626	??			0.017	0.007	11.1	0.81	–
79	RX J2117.7+5139	??			0.017	0.006	23.3	0.00	–
80	RX J2101.6+4730	AC	G0V	HD 200406	0.017	0.006	10.1	1.00	< 1.00
81	RX J2046.7+4728	AC?		? A =GSC-0357800892	0.017	0.006	9.2	0.98	–
82	RX J2136.6+4911	??			0.017	0.006	19.0	0.00	–
83	RX J2118.6+5010	AC	K0V	HD 203136	0.017	0.005	19.1	1.00	–
84	RX J2130.3+4709	CV	Me+DA	B	0.016	0.006	10.6	1.00	–
85	RX J2116.0+4827	??			0.016	0.006	8.9	0.00	–
86	RX J2124.7+4714	AC		A =GSC-0359402027	0.016	0.006	12.2	0.99	–
87	RX J2117.5+4330	AC	F8V	A =GSC-0318100914	0.016	0.006	8.7	0.99	0.73
88	RX J2137.6+4916	??			0.016	0.005	15.3	0.90	–
89	RX J2100.6+5039	AC		A =GSC-0360000197	0.016	0.006	9.1	0.99	–
90	RX J2119.5+4933	AC		A =GSC-0359201435	0.016	0.006	9.2	0.99	–

Table 12. Optical identifications for sources with $7 \leq \text{ML} \leq 8$. Entries are sorted by decreasing count rates. For the sake of completeness, we also list the proposed counterparts having a probability of identification in the range 95% - 98%. These more uncertain cases are marked by a '?' as first letter of the identification name and the class acronym is followed by a '?'

129	RX J2053.2+4951	??			0.020	0.008	7.9	0.00	—
130	RX J2054.0+4858	??			0.019	0.007	7.7	0.00	—
131	RX J2049.6+5128	AC	A =GSC-0358700147		0.017	0.008	7.3	0.99	—
132	RX J2052.3+4843	AC	A =GSC-0357901214		0.016	0.006	7.1	0.99	—
133	RX J2129.2+4604	??			0.016	0.006	7.9	0.00	—
134	RX J2124.5+5133	??			0.015	0.006	7.0	0.00	—
135	RX J2117.2+5241	AC	A =GSC-0395301223		0.014	0.006	7.9	0.99	—
136	RX J2057.6+4750	??			0.013	0.006	7.8	0.00	—
137	RX J2111.6+4809	CV	V1500 Cyg		0.013	0.005	7.6	1.00	—
138	RX J2051.8+4741	??			0.013	0.005	7.7	0.00	—
139	RX J2057.1+4929	??			0.013	0.005	7.9	0.00	—
140	RX J2043.1+4752	AC?	? A =GSC-0357802133		0.013	0.005	7.4	0.98	—
141	RX J2127.1+4801	??			0.012	0.005	7.5	0.00	—
142	RX J2048.8+4631	??			0.012	0.005	7.8	0.94	—
143	RX J2110.5+5244	??			0.011	0.005	7.8	0.00	—
144	RX J2052.3+4656	??			0.011	0.005	7.5	0.30	—
145	RX J2101.2+4609	OB	B1Ve	HD 200310	0.011	0.005	7.7	1.00	—
146	RX J2055.7+4815	??			0.011	0.005	7.3	0.00	—
147	RX J2045.1+4805	AC	A =GSC-0357800263		0.011	0.005	8.0	0.99	—
148	RX J2110.3+4832	??			0.011	0.004	7.5	0.00	—
149	RX J2131.2+4812	??			0.010	0.005	7.5	0.94	—
150	RX J2058.7+4845	??			0.010	0.004	8.0	0.00	—
151	RX J2100.3+4810	??			0.010	0.004	7.9	0.89	—
152	RX J2130.8+4842	??			0.009	0.004	7.1	0.00	—
153	RX J2052.6+4703	??			0.009	0.004	7.5	0.00	—
154	RX J2055.0+5039	??			0.009	0.004	7.4	0.00	—
155	RX J2121.1+4907	??			0.008	0.004	7.2	0.95	—
156	RX J2122.4+4709	??			0.008	0.004	7.3	0.93	—
157	RX J2054.6+4903	??			0.008	0.004	7.8	0.00	—
158	RX J2121.5+4951	??			0.006	0.003	7.5	0.00	—